CONICALLY SIMILAR SWIRLING FLOWS AT HIGH REYNOLDS NUMBERS

by R. FERNANDEZ-FERIA,

(*Universidad de Málaga, E.T.S.Ingenieros Industriales,* 29013 *Málaga, Spain*)

J. FERNANDEZ DE LA MORA,

(*Department of Mechanical Engineering, Yale University, New Haven, Connecticut* 06520-2159, *USA*)

M. PEREZ-SABORID *and* A. BARRERO

(*Universidad de Sevilla, E.T.S. Ingenieros Industriales,* 41012 *Sevilla, Spain*)

[Received 9 September 1997. Revises 8 December 1997 and 5 February 1998]

Summary

A new class of both inviscid and boundary layer self-similar solutions for conical swirling flows at high Reynolds numbers is analysed. For the case of one-cell solutions, the flow consists of an inviscid, but in general rotational, core with a velocity field, in spherical polar coordinates, of the form $\mathbf{u} = r^{m-2}\mathbf{V}(\theta)$, where m is any real number. Due to the known existence of two integrals to Euler's equations, the vector function $\mathbf{V}(\theta)$ is obtained by the integration of a second-order ordinary differential equation, containing the two integration constants K and K_1 associated with the intensities of the swirl and the meridional motion, respectively. This inviscid flow is, however, singular at the axis and must be regularized through a thin viscous layer, which also has self-similar structure. A variety of flow regimes are obtained for different ranges of m, all of them exhaustively analysed. In particular, for $0 < m < 2$, the solution to the near-axis boundary layer equations has the interesting property of losing existence when a certain inviscid swirl parameter, $D \sim K_1/K^4$, is either larger or smaller than a critical value, depending on m. We hypothesize that when this occurs, a two-cell flow structure develops. For $1 < m < 2$, we find that the two-cell structure consists of a thin fan-jet separating two inviscid regions; the flow in the outer cell being vortical while that in the inner one is potential. Flows of the two-cell type cannot exist for $0 < m < 1$. Transition from a one- to a two-cell solution is discussed with relevance to a simple example of vortex breakdown. In order to meet any given boundary condition on a certain cone surface $\theta = \alpha$ (or a plane for $\alpha = \frac{1}{2}\pi$), another viscous boundary layer is needed near it, which also has self-similar structure. In the most interesting range $0 < m < 2$, this boundary layer also regularizes the singular behaviour of the inviscid flow at the cone surface; in this range, the pressure gradient is negligible inside that boundary layer, allowing for an exhaustive two-dimensional phase space analysis. Two different boundary conditions are considered on the cone surface: a no-slip boundary condition, modelling the interaction of general conical vortices (at high Reynolds numbers) with a cone or a plane, and a shear stress varying as r^n. For this last boundary condition, three different relations between the powers n and m are obtained for three different inviscid flow regimes. This shear driven flow appears in some instances to model the motion inside so-called Taylor cones for which $n = -\frac{5}{2}$ ($m = \frac{10}{13}$).

1. Introduction

Exact solutions to either the Navier–Stokes (NS) equations or their nearly inviscid approximation are rare (for example, Wang (**1**)). But a few simple geometries have given the mathematician and the fluid dynamicist a rich ground for exploration of their properties. The particular case of incompressible flows whose velocity field **u** has polar symmetry of the form

$$\mathbf{u} = r^{m-2}\mathbf{V}(\theta), \tag{1}$$

where m is any real number, has been the subject of considerable attention, both in two dimensional as well as in three dimensional flows. For two dimensional situations with $m = 1$, exact solutions of the form (1) are possible for the full NS equations, such as in the Jeffery–Hamel flow inside converging and diverging channels (Jeffery (**2**), Hamel (**3**)). These flows are characterized by the possibility of separation, with the appearance of several cells in diverging channels. The corresponding richness of regimes discovered analytically is striking for such a simple geometry (for example, Goldshtik *et al.* (**4**)). Well known also are the two dimensional potential solutions of the form (1) to the Euler equations for $m = 1$, which are not exact NS solutions. Their corresponding boundary layer description (the so-called Falkner–Skan flows) illustrates analytically the role of positive pressure gradients in destabilizing and reversing locally the directions of such flows near walls. Interestingly enough, only irrotational solutions to the Euler equations and their corresponding boundary layers have been considered for flows of the type (1) with $m \neq 1$. Yet, this family of two dimensional flows is not necessarily restricted to potential situations. Furthermore, in the case when separation cells appear, it is clear that they must contain substantial vorticity. The interest of analysing two dimensional rotational flows of type (1) is therefore apparent, as shown in this work for three dimensional flows.

In the three dimensional case, the former *wedge* flows of type (1) become *conically symmetric*. The associated richness of allowed mathematical (and real) structures is now considerably increased for several reasons, including the possibility of swirl. An impressive show of the seemingly inexhaustible variety of associated mathematical behaviours has been already given in the literature for the case $m = 1$, which has been studied extensively at the NS level (Landau (**5**), Squire (**6**), Goldshtik (**7**), Yih *et al.* (**8**), Pillow and Paull (**9**), Paull and Pillow (**10**), Bojarevics *et al.* (**11**), Goldshtik and Shtern (**12**), Sozou (**13**), among others), as well as within the boundary layer approximation (for example, Taylor (**14**), Long (**15**), Burggraf *et al.* (**16**), etc.). Most interesting in this case is the appearance of either multiple solutions, singularities at the axis, solution breakdown, transitions from certain branches to others, etc., as the Reynolds number or the swirl intensity vary. Such behaviour is not only of great mathematical interest, but has been interpreted also as a hypothetical manifestation of certain poorly understood natural phenomena associated with swirling flows.

For instance, the near-axis problem for $m = 1$ was considered some time ago by Long (**15**) (Long's vortex), and a solution only exists for a particular combination of the swirl and meridional motion intensities characterized by the value $L = \sqrt{2}$, where L is defined as the ratio between the azimuthal and radial inviscid velocity components near the axis,

$$L \equiv |u_\phi / u_r|_{\theta \to 0}\,. \tag{2}$$

This restriction is imposed by the regularization of the inviscid solution at the axis through a viscous boundary layer. In this case, the relevant parameter that characterizes the near-axis solutions is the so-called *flow force* M, or non-dimensional total axial momentum flux, which is independent of the coordinate along the axis. Long found that for M smaller than a critical value M^*, no self-similar solution exists while for $M > M^*$ there are two possible solutions, which were termed by Burggraf and Foster (**17**) type I and type II solutions. These last authors sought numerical solutions to the near-axis boundary layer equations which matched to Long's inviscid asymptote, for given upstream conditions which did not necessarily coincide with those corresponding to self-similar solutions. They found that for values of the flow force M (fixed by the upstream conditions) larger than the critical value M^*, the boundary layer flow always evolved rapidly towards one of the two self-similar solutions (type II), but for $M < M^*$, when no self-similar solution exists, the viscous region readily invaded much of the flow field. Burggraf and Foster concluded that lack of existence of self-similar solutions to the boundary layer equations for a certain conical outer vortex implied that the viscous core could not be confined to a narrow axial region. The outer vortex could accordingly no longer survive and would necessarily break down. Thus, their study provided compelling evidence in favour of Hall's theory (for example, Hall (**18**)) associating vortex breakdown to the failure of the near-axis boundary layer equations.

The work by Shtern and Hussain (**19**) further clarified the picture for conically similar flows with $m = 1$. These authors found three branches of self-similar solutions to the Navier–Stokes equations forming a hysteresis loop with jump transitions between flow regimes. For high Reynolds numbers, two of these branches correspond, near the axis, to Long's solutions of type I and II, while the third one (type III solutions) corresponds to a *two-cell* flow where a viscous conical fan jet separates an inviscid, but rotational, outer cell from a potential inner cell. (This work has been recently extended by Shtern and Hussain (**20**) where new solution branches are found.) Interestingly enough, Shtern and Hussain found that, for decreasing M, a solution of type I jumps, when $M = M^*$, to a solution of type III with a two-cell flow structure. They have further related this phenomenon to vortex breakdown, which often gives rise to a bubble structure flow with recirculating motion and negligible swirl inside. They also found the opposite phenomenon of abrupt *vortex consolidation:* for increasing M, when M reaches another critical value, a solution of type III jumps to a type I solution, so that a two-cell flow suddenly reorganizes itself into a near-axis swirling jet.

For conical flows with $m \neq 1$, we also found solution loss of the near-axis boundary layer equations for nearly inviscid vortices (Fernandez-Feria, Fernandez de la Mora and Barrero (**21**)). In these cases, the flow force is no longer constant along the near axis viscous vortex, but the swirl parameter L plays a role somewhat analogous to M for Long's vortices: when $0 < m < 1$, two self-similar solutions exist for $L > L^*(m)$, and there is no solution for $L < L^*(m)$; when $1 < m < 2$, no solutions exist for $L > L^*(m)$, and there are two possible solutions for $L < L^*(m)$ (**21**, Fig. 3). These findings, in particular those for $1 < m < 2$, have a number of features in common with earlier numerical and experimental results for less idealized vortices (see, for example, Spall *et al.* (**22**) and Beran and Culik (**23**), among others). For instance, the relevant parameter governing vortex breakdown in real flows is not the flow force characterizing the transitions between branches in flows of type (1), but the swirl parameter L (or its inverse, a Rossby number, see, for example, (**22**)) arising in the otherwise analogous conical flows with $m \neq 1$. Furthermore, it is also shown in (**22**), (**23**) that, for high Reynolds numbers, the critical value of L above which vortex breakdown occurs is approximately equal to $\sqrt{2}$, which is the value found in (**21**) for conically similar flows with m slightly larger than unity. This coincidence suggests that most real vortices are (near the axis) not of the form $1/r$ but, rather, of the more general form (1), with m slightly larger than unity, as otherwise corroborated

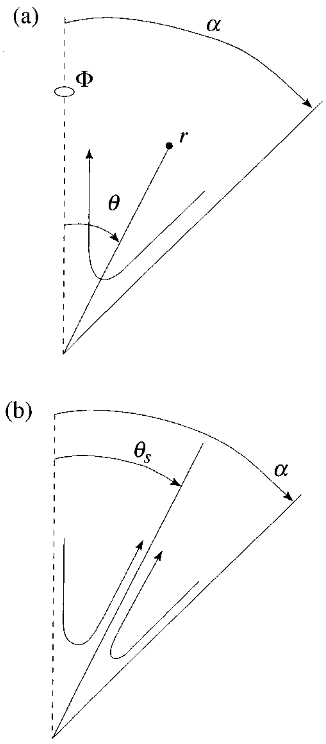

Fig. 1 Sketch of the one-cell (a) and two-cell (b) flows. Spherical coordinates are also shown

by many experimental data (for example, (**21**), (**22**)). This remarkable circumstance provides one justification for the analysis in detail of the class of steady, nearly inviscid swirling flows, which are conically similar solutions to the boundary layer approximation to the Navier–Stokes equations. We analyse in this work both one-cell and two-cell conically similar solutions (see sketches in Fig. 1).

We start in section 2 by deriving the general solution to the Euler equations with conical symmetry; that is, solutions for swirling inviscid flows with a velocity field which, in spherical polar coordinates (r, θ, ϕ), has the form (1). Known integrals to the Euler equations then reduce the problem to the integration of a second-order ordinary differential equation for the polar dependence $F(\theta)$ of the stream function for the meridional motion $\Psi \equiv r^m F(\theta)$. For each value of m, and for each of the two constants K and K_1 resulting from the two integrals of Euler's equations, a unique solution exists satisfying the boundary conditions that both the axis of symmetry and a certain conical surface of semiangle α are meridional streamlines. The two constants K and K_1 are related to the intensities of the swirl and the meridional motion, respectively. The inviscid flow is in general rotational, except for the case when $K = K_1 = 0$; the case when $K = 0$ and $K_1 \neq 0$ (non-potential flow without swirl velocity component) is treated separately in Appendix B.

When $0 < m < 2$, the inviscid flows thus found are singular at the axis of symmetry as well as at the outer streamline of the cone $\theta = \alpha$ (except for potential flows), and must be regularized. The corresponding viscous boundary layer at the axis has also a self-similar structure, which is *richer* in the interval $0 < m < 2$ (analysed in (**21**)) than for $m \leq 0$ and $m > 2$ (section 3). In the former case, the regularizing boundary layer exists only within certain ranges of values of L, as just discussed. This excludes, for instance, non-swirling flows for $0 < m \leq 1$, and purely swirling flows for $1 < m < 2$. When this type of solution breakdown occurs, the one-cell type solution ceases to be valid. We hypothesize that the flow then jumps to a two-cell structure, analogous to that discussed by Shtern and Hussain (**19**) for $m = 1$, which is analysed in sections 6 and 7.

Before that, in order to either interpret the singularity appearing at the cone surface ($\theta = \alpha$) when $0 < m < 2$, or otherwise to be able to impose physically meaningful boundary conditions at this boundary, we analyse in sections 4 and 5 the viscous boundary layer needed at $\theta = \alpha$ for the cases in which its structure is self-similar. Since it is shown in section 2 that the inviscid azimuthal component is negligible in comparison with the radial one near the cone surface, the surface boundary layer equations for the meridional motion are decoupled, at first approximation, from the azimuthal equation, and only those are considered in sections 4 and 5 (the swirl boundary layer equation is analysed in Appendix C). Interestingly enough, we also find in section 2 that, for $0 < m < 2$, and for any value of m if the inviscid flow is potential ($K = K_1 = 0$), the pressure is also negligible compared to the dynamical pressure inside the boundary layer at the cone surface. Thus, the boundary layer analysis is substantially simplified for these cases, allowing for an exhaustive two dimensional phase space description, which is carried out in section 4. This analysis provides a complete picture of all the possible self-similar solutions to the boundary layer equations and, therefore, of all the possible boundary conditions on the cone surface compatible with the inviscid conical flows. Of these, we shall consider two physically important cases: the no-slip boundary condition, with regularizes the inviscid conical flow over a conical solid wall (or over a flat plate for $\alpha = \frac{1}{2}\pi$), and a shear stress acting on the surface of the cone of the form

$$\tau_{r\theta} = j\Gamma_n r^n, \qquad j = \pm 1, \tag{3}$$

where Γ_n (> 0) and n are constants (of course, the power n is related to m; see sections 4 and 5). With the first boundary condition, this paper contributes to the problem of the existence of self-similar boundary layer solutions for the interaction of an inviscid vortex with a cone or a plane (for example, Taylor (**14**), Burggraf *et al.* (**16**), Belcher *et al.* (**24**), Sozou (**13**)). The conical flows produced by the second class of boundary conditions provide a model for the liquid motion observed inside electrified menisci, generally called Taylor cones. Such conical menisci appear at the interface between a gas and a conducting liquid charged to a high electrical potential. A free conical surface forms then as a stable structure. Furthermore, due to tangential electric fields, shear stresses pointing towards the cone apex ($j = -1$) appear always along the surface (for example, Hayati *et al.* (**25**)). A reliable comparison between model predictions and experimental observations of circulating flows inside Taylor cones is not possible at this stage due to the absence of a complete theory of the fields and currents inside the cone. However, the conical symmetry of this problem gives strong indications that indeed the shear stress at the surface follows a power law with r. This is shown by a variety of existing models for the Taylor cone (none of which is free from inconsistencies). For instance, the surface charge density scales in Taylor's theory as $r^{-1/2}$, while the radial electric field varies as r^{-2} for relatively conducting liquids (Gañán-Calvo (**26**); see also Fernandez de la Mora and Loscertales (**27**) and Gañán-Calvo *et al.* (**28**), for a discussion). The power n in (3) would then be $-\frac{5}{2}$, corresponding to $m = \frac{10}{13}$, and, therefore, a value of m different from unity. In addition to these two physical problems, the solutions depicted in the phase plane for $0 < m < 2$ are also essential to describe the conical fan-jet appearing in the two-cell flows (section 8).

For $m \leq 0$ and $m \geq 2$, the viscous flow is regular at the cone surface, but a viscous boundary layer is still needed there to meet the same boundary conditions on the cone surface used in section 4. The corresponding analysis, given in section 5, is not so rich and simple as in the range $0 < m < 2$. Indeed, because the pressure gradient term is not negligible inside the boundary layer, the problem cannot be reduced to the analysis of just one first-order ordinary differential equation, very much as in the Falkner-Skan problem.

In section 6 we summarize and discuss all the possible *one-cell* conically similar solutions compatible with a no-slip boundary condition, and with a shear stress boundary condition of the form (3). Solutions describing *two-cell* flows are analysed in sections 7 and 8. These flows appear, we conjecture, when breakdown of the one-cell type solution occurs above (below) a critical value of the swirl parameter for $1 < m < 2$ $(0 < m < 1)$. Actually, we show there that two-cell conically similar solutions exist only for $1 \leq m < 2$. The flow structure described by a two-cell type solution is a generalization to values of $m \neq 1$ of that given by Shtern and Hussain (**19**) . It consists of a conical fan jet (section 8) separating an inviscid, but rotational, outer cell from a potential inner cell (section 7). Section 9 discusses two-cell solutions and their possible relation to vortex breakdown. Concluding remarks are given in section 10.

2. Conically similar inviscid flows

We present in this section the general class of conically similar solutions to the steady Euler equations for an incompressible fluid. We look for solutions where the velocity field **u** depends on the variables r and θ as in (1). In terms of the stream function for the meridional motion Ψ,

$$\Psi \equiv r^m F(x), \quad x = \cos\theta, \tag{4}$$

through which the continuity equation is automatically satisfied, one has

$$u_r = -r^{m-2}F'(x), \quad u_\theta = -mr^{m-2}F(x)/(1-x^2)^{1/2}, \tag{5}$$

where primes denote differentiation with respect to x. We define the additional swirl and pressure functions Ω and Π:

$$u_\phi \equiv r^{m-2}\Omega(x)/(1-x^2)^{1/2}, \quad p/\rho \equiv r^{2(m-2)}\Pi(x), \tag{6}$$

so that the Euler momentum equations become

$$mFF'' - (m-2)(2\Pi + F'^2) + \frac{m^2F^2 + \Omega^2}{1-x^2} = 0, \tag{7}$$

$$mFF' + \frac{x}{1-x^2}(\Omega^2 + m^2F^2) + (1-x^2)\Pi' = 0, \tag{8}$$

$$(m-1)\Omega F' = mF\Omega'. \tag{9}$$

Equation (9) may be integrated immediately into

$$\Omega = K|F|^{(m-1)/m}, \tag{10}$$

where K is an arbitrary constant.† This first integral is related to Kelvin's circulation theorem for a circular path where both r and θ are constants (see below). Another first integral of (7) to (9), related to Bernoulli's law, may be obtained by writing (8) as

$$\left[\Pi + \frac{m^2F^2+\Omega^2}{2(1-x^2)}\right]' = -\frac{mF^2}{1-x^2}\frac{F'}{F} + \frac{(m^2F^2+\Omega^2)'}{2(1-x^2)}. \tag{11}$$

Expanding the right-hand side of this equation making use of (9), and adding $(F'^2)'/2$ to both sides, one arrives at

$$\left[\Pi + \frac{F'^2}{2} + \frac{m^2F^2+\Omega^2}{2(1-x^2)}\right]' = \frac{m-1}{m}\frac{m^2F^2+\Omega^2}{1-x^2}\frac{F'}{F} + F'F''. \tag{12}$$

On the other hand, multiplying (7) by F'/mF,

$$F'F'' = \frac{m-2}{m}(2\Pi + F'^2)\frac{F'}{F} - \frac{m^2F^2+\Omega^2}{m(1-x^2)}\frac{F'}{F}, \tag{13}$$

and substituting into (12), one obtains

$$\left[\Pi + \frac{F'^2}{2} + \frac{m^2F^2+\Omega^2}{2(1-x^2)}\right]' = 2\frac{m-2}{m}\frac{F'}{F}\left[\Pi + \frac{F'^2}{2} + \frac{m^2F^2+\Omega^2}{2(1-x^2)}\right]. \tag{14}$$

This equation is straightforwardly integrated into

$$2\Pi + F'^2 + \frac{m^2F^2+\Omega^2}{1-x^2} = \text{constant} \times F^{2-4/m} \equiv \frac{K_1}{m-2}F^{2-4/m}, \tag{15}$$

where K_1 is another arbitrary constant.

Substituting (10) and (15) into (7) one obtains the second-order differential equation

$$mF'' + (m-1)\frac{m^2F + K^2F^{1-2/m}}{1-x^2} = K_1F^{1-4/m}. \tag{16}$$

This equation will be solved with the boundary conditions that the axis of symmetry and the cone surface, situated at a certain angle $\theta = \alpha$, are parallel to the flow; that is,

$$F(1) = F(\cos\alpha) = 0. \tag{17}$$

(For potential flows (section 2.2), the second boundary condition will be relaxed to $F(\cos\alpha) =$ constant.) Some analytic solutions to this problem for specific values of m are given in Appendix A.

This considerably reduced formulation is a special case of the known representation of

† For simplicity, we shall use F (> 0) for $|F|$; notice that if (F, Ω, Π) is a solution to equations (7) to (9), $(aF, \pm a\Omega, a^2\Pi)$ is also a solution for any real number a. In particular, an inviscid flow with the meridional motion inverted in relation to the one considered in what follows (that is, $a = -1$) is also a solution of the problem, independently of the sense of the swirl.

Euler's equations for steady axisymmetric situations, where rotational invariance and energy conservation hold independently of the more restrictive requirement of conical symmetry imposed here. In spherical coordinates, the corresponding equation for the stream function may be written as

$$\frac{\partial^2\Psi}{\partial r^2} + \frac{1}{r^2}\frac{\partial^2\Psi}{\partial\theta^2} - \frac{\cot\theta}{r^2}\frac{\partial\Psi}{\partial\theta} = r^2\sin^2\theta\frac{dH}{d\Psi} - C\frac{dC}{d\Psi}, \tag{18}$$

where the two Lagrangian constants of motion

$$C \equiv \frac{1}{2\pi}\oint \mathbf{u}\cdot\mathbf{dr}, \quad H \equiv \tfrac{1}{2}\mathbf{u}\cdot\mathbf{u} + \frac{p}{\rho}, \tag{19}$$

depend only on Ψ.† For the present case, it follows from (4) to (6) and (19) that

$$C = r^{m-1}\Omega = K\Psi^{(m-1)/m}, \quad H = r^{2(m-2)}\left[\Pi + \tfrac{1}{2}F'^2 + \frac{m^2F^2+\Omega^2}{2(1-x^2)}\right] = \frac{K_1}{2(m-2)}\Psi^{2(m-2)/m}; \tag{20}$$

that is, (10) and (15). Equation (16) is then obtained from (18) straightforwardly.

2.1 *Description of the solutions*

One of the two constants K and K_1 may be absorbed into a new dimensionless dependent variable Y through the definitions

$$Y = F/K^m, \quad D = -2m^2K_1/K^4, \tag{21}$$

which transform (16), (17) into

$$mY'' + (m-1)\frac{m^2Y + Y^{1-2/m}}{1-x^2} = -\frac{D}{2m^2}Y^{1-4/m}, \tag{22}$$

$$Y(1) = Y(\cos\alpha) = 0. \tag{23}$$

The case $K = 0$ must be treated separately. The corresponding analysis differs only slightly from the following one for $K \neq 0$, except for potential flows ($K_1 = K = 0$), which are analysed in section 2.2 below. (The case $K = 0$ with $K_1 \neq 0$, that is, the case of non-potential swirl-less flows, is analysed in Appendix B.) Notice in (15) that $K_1/(m-2) > 0$, so that the ratio D between the intensity of the meridional motion (K_1) and the swirl intensity (K) must be positive for $m < 2$, and negative for $m > 2$ (an analytic solution is given in Appendix A for $m = 2$).

The initial and final points of the integration domain $\cos\alpha \leq x \leq 1$ for (22) are singular as a result of the boundary conditions (23). The behaviour of Y in their vicinity determines the structure of the two viscous boundary layers arising at both ends (the cone surface and the axis). As we shall see, the character of the singular points changes at $m = 0$ and $m = 2$, in such a way that for $0 < m < 2$ the pressure gradient has a negligible effect on the boundary layer at the cone surface, while this feature is lost for $m \leq 0$ and $m \geq 2$. Due to the essentially different natures of the solutions in these ranges of values of m, they will be analysed separately. The limiting cases $m = 0$ and $m = 2$ are solved in closed forms in Appendix A.

† The cylindrical version of (18) is usually called the Bragg–Hawthorne equation after (**29**); however, according to a reviewer, the equation was used before by E. Meissel (*Archiv der Mathematik und Physik* **55** (1873)).

2.1.1 $m < 0$. In this case one has the following near-axis behaviour:

$$Y = a_1(1-x)\left[1 + \tfrac{1}{4}m(1-m)(1-x) + O((1-x)^2)\right], \tag{24}$$

where a_1 is an arbitrary constant. Putting $a_1 > 0$ and proceeding numerically away from the axis (which is a saddle) one finds that Y eventually vanishes again, fixing the cone angle at a certain $\theta = \alpha(a_1)$. Linear analysis shows that the solutions approach this point as

$$Y \to B_1(x - \cos\alpha), \quad x \to \cos\alpha, \tag{25}$$

where B_1 is a constant which depends on α and, therefore, on a_1. Some solutions with $m = -1$ and $D = 2$ are given in Fig. 2(a) for different values of α.

According to (24) and (25), the behaviour of the velocity field and pressure near the axis and at the surface of the cone are, respectively,

$$x \to 1\,(\theta \to 0): \quad \Psi \to a_1(Kr)^m \frac{\theta^2}{2}\left(1 + \frac{3(1-m)m-2}{24}\theta^2\right), \tag{26}$$

$$u_\phi \to K^m (a_1/2)^{(m-1)/m} (r^m\,\theta)^{(m-2)/m}, \tag{27}$$

$$p/\rho \to -\tfrac{1}{2}a_1^2 K^{2m} r^{2(m-2)}\left(1 + \tfrac{1}{4}m(2-m)\,\theta^2\right); \tag{28}$$

$$x \to \cos\alpha: \quad \Psi \to B_1(Kr)^m(x - \cos\alpha), \tag{29}$$

$$u_\phi \to \frac{K^m B_1^{(m-1)/m}}{\sin\alpha} r^{m-2}(x - \cos\alpha)^{(m-1)/m}, \tag{30}$$

$$p/\rho \to -(K^m B_1)^2\, r^{2(m-2)}/2. \tag{31}$$

Note that the velocity field and the pressure are regular at the axis. However, we shall see in section 3.2 that viscosity cannot be neglected in a narrow region near the axis, where only u_ϕ is modified at the lowest order; the meridional velocity components and the pressure are affected by viscosity at the next order which, for that reason, is included in the expressions (26) and (28). On the other hand, near the cone surface, the radial velocity is regular and does not depend on $x - \cos\alpha$,

$$u_r \to -B_1 K^m r^{m-2}, \tag{32}$$

though a viscous boundary layer is needed at the cone surface in order to accommodate any externally imposed boundary condition. In that boundary layer one may neglect u_ϕ in the radial momentum equation because, from (29) and (30), $u_\phi/u_r \sim (x - \cos\alpha)^{(m-1)/m} \to 0$ as $x \to \cos\alpha$ (see sections 4 and 5). Finally, as $x \to \cos\alpha$, the pressure gradient is of the same order as the convective terms, $\partial p/\partial r \sim \rho u_r \partial u_r/\partial r$, so it should be retained in the boundary layer near the cone surface when $m < 0$.

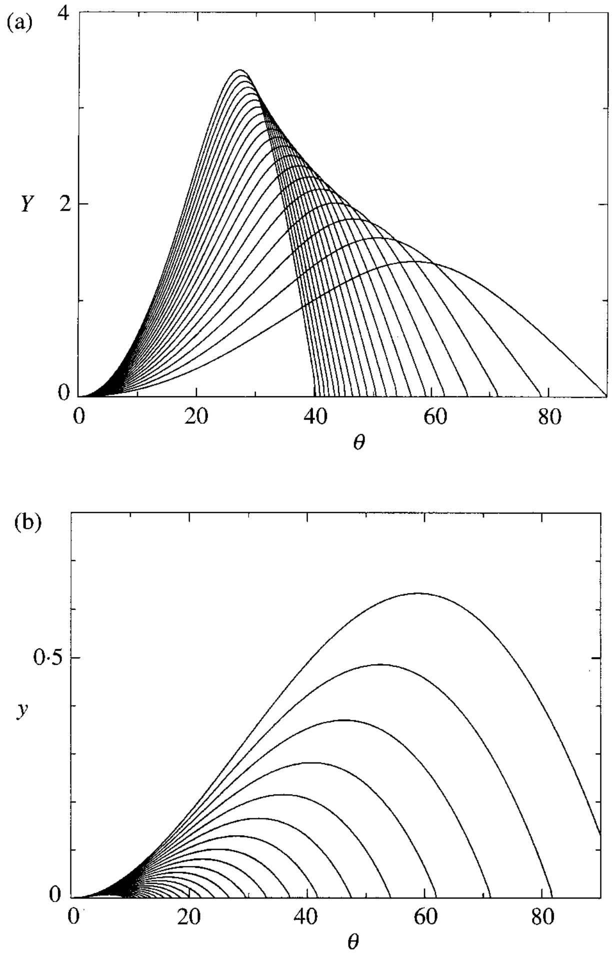

Fig. 2 (a) $Y(\theta)$ for $m = -1$ and $D = 2$ for some values of the cone angle α. (b) $y(\theta) = m^2 Y(\theta)^{2/m}$ for $m = \frac{8}{5}$ ($n = -1$) and $D = 1$ for several values of α

2.1.2 $0 < m < 2$. In this case, it is convenient to use the new variable

$$y = m^2 Y^{2/m}, \tag{33}$$

which transforms (22), (23) into

$$yy'' + \frac{m-2}{2} y'^2 + \frac{2(m-1)}{1-x^2}(y^2 + y) + D = 0, \tag{34}$$

$$y(1) = y(\cos\alpha) = 0. \tag{35}$$

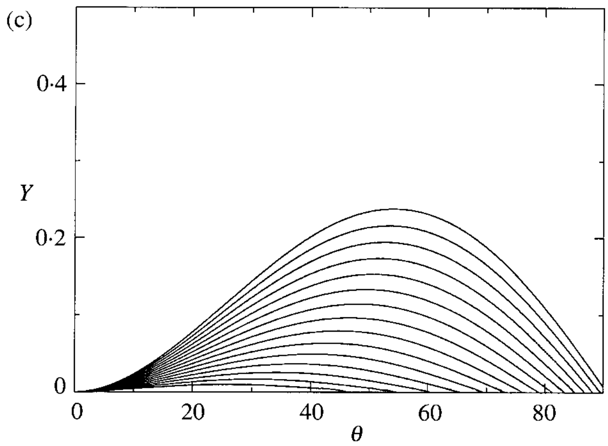

Fig. 2 (c) $Y(\theta)$ for $m = \frac{5}{2}$ and $D = -1$ for some values of the cone angle $\alpha > \alpha^* \sim 40^\circ$

Further, (34) may be reduced to the first-order differential equation

$$\frac{d\Sigma}{d\sigma} = \frac{-D - (m-1)\sigma - (m-2)\Sigma^2/2}{\sigma(\Sigma - \sigma)} \tag{36}$$

in terms of the new variables

$$\chi = 1 - x, \quad \sigma = y/\chi, \quad \Sigma = dy/d\chi. \tag{37}$$

Three possible stationary points of (36) arise, either with $\sigma = 0$ and $\Sigma = [2D/(m-2)]^{1/2}$; or with $\Sigma = 2\sigma/m \to \infty$; or with $\Sigma = \sigma = 2a$, where a is the positive root of

$$(m-2)a^2 + (m-1)a + D/2 = 0. \tag{38}$$

In the case $\sigma = 0$, the requirement that the numerator of (36) vanishes, forces Σ to be different from zero, which is incompatible with the starting condition $(\chi, y) = (0, 0)$ and (37). The case $\Sigma = 2\sigma/m \to \infty$ is the appropriate initial point when $m > 2$ (see section 2.1.3). For the case $0 < m < 2$ the appropriate starting point is $\Sigma = \sigma = 2a$. Linearizing (36) in its vicinity and integrating shows that

$$y = 2a(1-x)[1 + A(1-x)^{\lambda^+} + B(1-x)^{\lambda^-}] + O(y^2), \tag{39}$$

where λ^+ and λ^- are the roots of

$$\lambda^2 + \lambda(m-1) + m - 2 + (m-1)/(2a) = 0. \tag{40}$$

Since $(2-m)D > 0$ for $m < 2$, it is shown that λ^+ and λ^- are real and have opposite signs. Thus, the point $\Sigma = \sigma = 2a$ is an unstable saddle, and the axis can only be reached through the special family of trajectories where $B = 0$ in equation (39).

On the other hand, near the cone surface, (22) may be integrated once into

$$Y'^2 = \frac{D}{(2-m)2m^2} Y^{2(m-2)/m} + Gm^{2(2-m)} - \frac{Y^{2(m-1)/m}}{\sin^2 \alpha} + O(Y^2), \tag{41}$$

where G is also a free constant, and D is non-negative for $m < 2$, as shown above. Given certain values of A, D and m, one must start the numerical integration of equation (34) near the axis $x = 1$ (a saddle) with behaviour (39) with $B = 0$, and proceed further until the cone surface (a node) is reached; there, y (and Y) vanishes again with behaviour (41) at an angle $\alpha = \alpha(A, D, m)$ with $G = G(A, D, m)$. Figure 2(b) shows some solutions $y(\theta)$ for several values of A (or the cone angle), for the case $m = \frac{8}{5}$ with $D = 1$. When $A = 0$ the 'cone' angle is π and the solution is given analytically by $y = a(1 - x^2)$.

The velocity and pressure when approaching both the axis and the cone surface are

$$x \to 1\, (\theta \to 0): \quad \Psi \to (Kb\theta r)^m, \quad b \equiv a^{1/2}/m, \tag{42}$$

$$u_\phi \to K^2 b (Kb\theta r)^{m-2}, \tag{43}$$

$$\frac{p}{\rho} = \frac{K^4 b^2}{2(m-2)} (Kb\theta r)^{2(m-2)}; \tag{44}$$

$$x \to \cos\alpha: \quad \Psi \to (rKQ/m)^m (x - \cos\alpha)^{m/2}, \quad Q^4 \equiv 2D/(2-m), \tag{45}$$

$$u_\phi \to \frac{K^m (Q/m)^{m-1} r^{m-2}}{\sin\alpha} (x - \cos\alpha)^{(m-1)/2}, \tag{46}$$

$$p/\rho = -(G/2) K^{2m} m^{2(1-m)} r^{2(m-2)}. \tag{47}$$

Notice that the pressure has regular behaviour at the cone surface, while the radial velocity is singular in this range $0 < m < 2$. As a result the pressure p is negligible near $\theta = \alpha$ in relation to ρu_r^2, and the pressure gradient term may be neglected in the boundary layer at the cone surface (see section 4). More precisely, from (45) and (47), the pressure p is of the order $(x - \cos\alpha)^{2-m}$ for $\theta \to \alpha$ with respect to ρu_r^2, which goes to zero for $0 < m < 2$. Similarly, $(u_\phi/u_r)^2 \sim (x - \cos\alpha)$ near the surface, so that it is valid to neglect the terms proportional to u_ϕ in the radial momentum equation of the boundary layer at the surface (section 4). Equation (42) predicts that the radial velocity and its derivatives with respect to θ are singular at the axis for $0 < m < 2$, so that viscosity cannot be neglected near the axis.

2.1.3 $m > 2$. This case is very similar to that for $m < 0$. When $m > 2$, both roots λ^+ and λ^- of (40) are negative, so that the constant A in (39) must be equal to zero. Then, the behaviour near the point $x = 1$ changes, though it is still a saddle. Numerically one must start the integration of (22) as

$$Y \simeq a_2(1-x)\left[1 - \frac{m}{4(m-2)} a_2^{-2/m} (1-x)^{1-2/m}\right], \tag{48}$$

where a_2 is another free constant, analogous to a_1 and A defined earlier. The solution approaches

$x = \cos\alpha$ as (41) but, now, the second term dominates, and another integration yields

$$Y = m^{1-m} G^{1/2}(x - \cos\alpha). \tag{49}$$

When approaching the surface from its interior, the numerical integrations are also stable (as in the case $0 < m < 2$) provided that $G \neq 0$. When $G = 0$, the first term in (41) dominates as in the case $0 < m < 2$, though now this singular point is an unstable saddle. (This case is of interest for describing two-cell flows; see sections 7 and 8.) Given m and D (which for $m > 2$ should be negative), G is determined, similarly to the case $0 < m < 2$, as a function of a_2 (or α). A particular value of the cone angle α^* exists, for each m and D, for which $G = 0$, such that no solution exists with $\alpha < \alpha^*$ (see Fig. 2(c) for $m = 2{\cdot}5$ and $D = -1$). For $\alpha = \alpha^*$ the solution has the same behaviour as for $0 < m < 2$ (equation (41)). For $\alpha > \alpha^*$, G is positive and the solution approaches (49).

When $m > 2$, the behaviours of the solution near the axis and the cone surface are (for $G > 0$):

$$x \to 1(\theta \to 0): \quad \Psi \to a_2(Kr)^m \frac{\theta^2}{2}\left[1 - \frac{m}{8(m-2)}\left(\frac{a_2}{2}\right)^{-2/m} \theta^{2(m-2)/m}\right], \tag{50}$$

$$u_\phi \to K^m (a_2/2)^{(m-1)/m} (r^m\,\theta)^{(m-2)/m}, \tag{51}$$

$$\frac{p}{\rho} \to -\frac{a_2^2 K^{2m}}{2} r^{2(m-2)} \left[1 - \frac{m}{4(m-2)}\left(\frac{a_2}{2}\right)^{-2/m} \theta^{2(m-2)/m}\right]; \tag{52}$$

$$x \to \cos\alpha: \quad \Psi \to m\, G^{1/2} (Kr/m)^m (x - \cos\alpha), \tag{53}$$

$$u_\phi \to \frac{K^m G^{(m-1)/2m}}{m^{m-1}\sin\alpha} r^{m-2} (x - \cos\alpha)^{(m-1)/m}, \tag{54}$$

$$p/\rho \to -(G/2) K^{2m} m^{2(1-m)} r^{2(m-2)}. \tag{55}$$

The derivative of u_ϕ is singular at the axis, so that a near-axis viscous boundary layer should regularize that behaviour. The structure of this boundary layer is analogous to that for $m < 0$, and it is considered in section 3.2. Near the cone surface, u_r does not depend on x, and $u_\phi/u_r \sim (x - \cos\alpha)^{(m-1)/m} \to 0$ as $x \to \cos\alpha$, so that u_ϕ does not enter in the boundary layer at the cone surface (section 5). The pressure gradient is no longer negligible in that boundary layer.

2.2 *Potential flows*

Due to their qualitatively different features, potential flows have to be treated separately.

If $\mathbf{u} = \nabla\Phi$, because $\mathbf{u}$ itself does not depend on the azimuthal angle ϕ, the potential Φ can only be a linear function of ϕ with a proportionality coefficient which turns out to be the circulation: $\Phi = \varphi(r,\theta) + 2\pi C\phi$. If one further imposes the condition of conical symmetry, the term proportional to ϕ can only exist in the case $m = 1$, so that there cannot be any potential conical swirl when $m \neq 1$. The meridional flow corresponds to the solution to Laplace's equation with conical symmetry, given in terms of the Legendre functions P,

$$\varphi = A r^{m-1} P_{m-1}(\cos\theta), \tag{56}$$

which is regular at $\theta = 0$. The general solution (56) corresponds exactly with our results above for the special case when both $K = 0$ (there is no irrotational swirl except for $m = 1$) and $K_1 = 0$ (Bernoulli's constant is spatially uniform in steady irrotational problems). Then, (16) turns into

$$(1 - x^2)F'' + m(m - 1)F = 0, \tag{57}$$

which is equivalent to Legendre's equation for P (see, for example, Abramowitz and Stegun (**30**, 22.6.13)), after using the definitions for the velocity vector in terms of both F and P_{m-1}; if the condition $F(x = 1) = 0$ is imposed, these two functions must be related via

$$F = c(1 - x^2)P'_{m-1}, \tag{58}$$

where c is an arbitrary constant. In terms of P_{m-1}, the velocity field and pressure are given by

$$u_r = cm(m - 1)r^{m-2}P_{m-1}(x), \quad u_\theta = -cmr^{m-2}(1 - x^2)^{1/2}P'_{m-1}(x), \tag{59}$$

$$p/\rho = -\tfrac{1}{2}c^2m^2r^{2(m-2)}[(m - 1)^2P^2_{m-1}(x) + (1 - x^2)P'^2_{m-1}(x)]. \tag{60}$$

This solution is regular at the axis, so that no viscous boundary layer is needed there. For the case $m = 1$, the most general solution is $F = a + bx$, which cannot vanish at any other angle $\theta = \alpha$ if it vanishes at $\theta = 0$. In general, for any value of m, one has no freedom to impose the boundary condition $F(\cos\alpha) = 0$. However, it will be shown that the behaviour as $x \to \alpha$,

$$F(\cos\alpha) = \text{constant} \equiv c\sin^2\alpha\ P'_{m-1}(\cos\alpha), \tag{61}$$

matches with one of the trajectories of the phase plane that describes the solutions for the boundary layer at the cone surface analysed in section 4. Thus, among the inviscid flows considered here, potential flows are the only ones for which there exists an inviscid mass flux that is balanced by a viscous mass flux at the surface boundary layer. It must be noticed that, although from (59) and (60) the inviscid values of p/ρ and u_r^2 are of the same order as $x \to \alpha$, they are both negligible compared to u_r^2 within the boundary layer at the cone surface (see section 4.1.3).

3. Boundary layer at the axis

Euler's equations predict that, except for potential flows, the radial velocity and its derivatives with respect to θ are singular at the axis for $0 < m \leq 2$, as given by equation (42) (see Appendix A for $m = 2$). Alternatively, the derivatives of u_ϕ are singular when $m < 0$ or $m > 2$ (for $m = 0$, u_ϕ is singular at the axis; see Appendix A). Therefore, even at very high Reynolds numbers, it is inconsistent within the framework of the Navier–Stokes equations to ignore viscosity in a certain narrow region near the axis. The boundary layer analysis for the range $0 < m < 2$ is given in (**21**) (it must be noted that polar cylindrical coordinates are used in that work, instead of the spherical coordinates used here, because near the axis one has cylindrical rather than spherical symmetry). Its main results are summarized in section 3.1. Section 3.2 considers the boundary layer solutions for $m < 0$ and $m > 2$. The cases $m = 0$ and $m = 2$ are given in Appendix A.

3.1 *Case* $0 < m < 2$

Because the matching conditions (42) to (44) involve simple power laws and there are no external characteristic lengths, the boundary layer problem has a self-similar structure. It is shown in (**21**)

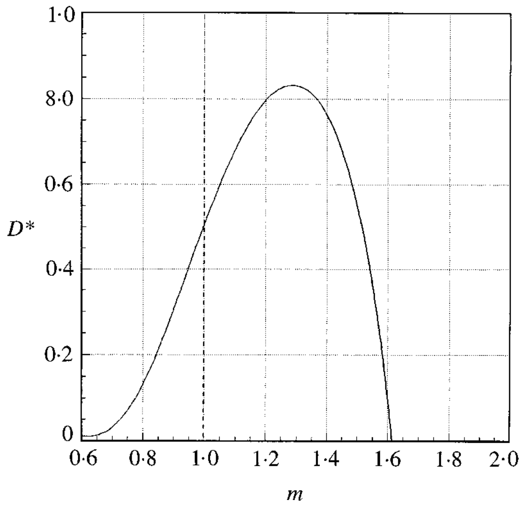

Fig. 3 Boundary $D^*(m)$ of the region of existence of solution for the near axis boundary layer, which is above the curve for $m > 1$ and below it for $m < 1$. For $m = 1$ the only allowed value is $D = \frac{1}{2}$, and no solutions exist for $m < 0.6$, approximately

that solutions to the boundary layer equations exist only for certain m-dependent ranges of the swirl parameter L, defined as the ratio between the azimuthal and the radial inviscid velocity components near the axis (equation (2) on using (42) and (43)):

$$L \equiv |u_\phi/u_r|_{\theta\to 0} = (mb)^{-1}; \tag{62}$$

L is related to the inviscid parameter D through (see (38) and (42))

$$L = (mb)^{-1} \equiv a^{-1/2} = \left[\frac{m-1}{2(2-m)} + \left(\frac{(m-1)^2}{4(2-m)^2} + \frac{D}{2(2-m)}\right)^{1/2}\right]^{1/2}, \tag{63}$$

(recall that $D > 0$ for $m < 2$). This parameter plays an important role in vortex flows because the known condition for high Reynolds number vortex breakdown was shown by Spall *et al.* (**22**), among others, to be that the ratio u_ϕ/u_r at the edge of the viscous core of the vortex is larger than a certain value near 1·5. Figure 3 in (**21**) shows the boundaries of existence of solution in (L, m)-space, $L^*(m)$. For $m > 1$, solutions exist only below the curve, so that the swirl cannot exceed an m-dependent maximum value given by that curve. For $m < 1$, the domain of existence is above the curve, and the swirl must be larger than a minimum value. For $m = 1$, all solutions are characterized by $L = \sqrt{2}$. Therefore, flows with an arbitrarily small swirl are allowed only for $m > 1$, and flows involving mostly pure rotation may exist only for $m < 1$. Figure 3 shows the existence of corresponding boundaries of solution in (D, m) space, $D^*(m)$. For $m > 1$, solutions only exist above the curve; for $m < 1$, the domain of existence is below the curve, and for $m = 1$, all solutions correspond to $D = \frac{1}{2}$.

For each value of L (or D) for which boundary layer solutions exist, two different solutions arise, which are equivalent to the types I and II defined by Burggraf and Foster (**17**) in relation to

Long's vortex (case $m = 1$). However, for the case $m = 1$, the intensities of the meridional and azimuthal motions are coupled for all solutions through $L = \sqrt{2}$ ($D = \frac{1}{2}$), and the parameter characterizing the different solutions is the non-dimensional flow force M, instead of L (see the Introduction). Two solutions (types I and II) exist when $M < M^*$ ($\simeq 3{\cdot}75$), and none may be found for $M > M^*$. For values of L (or M if $m = 1$) for which no near-axis boundary layer solutions exist, the one-cell flow considered in this paper ceases to be valid, and a *two-cell* flow arises. Its structure is described in sections 7 and 8 (see Shtern and Hussain (**19**) for the case $m = 1$).

Another important result obtained in (**21**) is that no solutions to the near-axis boundary layer equations exist when the inviscid meridional motion near the axis points towards the cone apex, which corresponds to $j = +1$ in (3) for shear driven flows. This does not happen for the cases $m \leq 0$ and $m \geq 2$ considered next, for which both directions are possible for the meridional motion (see the footnote on p. 7).

3.2 *Cases $m < 0$ and $m > 2$*

The type of singularity arising in these cases is relatively mild in comparison with $0 < m < 2$, because the inviscid meridional flow field is analytical at $\theta = 0$, and only the swirl velocity requires regularization near the axis at the lowest order. Since the boundary layer structure is analogous for $m < 0$ and $m > 2$, only the case $m > 2$ will be considered here.

The substitution of behaviours (50) to (52) into the near-axis boundary layer approximation of the Navier–Stokes equations shows that the viscosity terms become comparable to the inertial terms in a thin layer of angular thickness

$$\Delta \sim \left(\nu r^{m-1}/K^m\right)^{\frac{1}{2}} \ll 1. \tag{64}$$

However, viscosity does not affect the three velocity components in the same way: it leaves unaffected the lowest-order terms in the near-axis expansion of the inviscid meridional velocity components and pressure (equations (50) and (52)), modifying only the lowest-order term of the azimuthal velocity component (equation (51)), and the first orders in (50) and (52). This suggests the introduction of the following scaling and self-similar variables inside the near-axis boundary layer:

$$\eta = \theta/\Delta, \quad \Delta^2 = \nu r^{1-m}/K^m a_2, \tag{65}$$

$$\Psi = \frac{a_2 K^m}{2} r^m \theta^2 [1 - C\Delta^{2-4/m} f(\eta)], \quad C \equiv \frac{m}{8(m-2)} \left(\frac{a_2}{2}\right)^{-2/m}, \tag{66}$$

$$u_\phi = K^m \left(\tfrac{1}{2}a_2\right)^{(m-1)/m} \Delta^{1-2/m} r^{m-2} w(\eta), \quad p/\rho = -\tfrac{1}{2}a_2^2 K^{2m} r^{2(m-2)} [1 - 2C\Delta^{2-4/m}\beta(\eta)], \tag{67}$$

through which the boundary layer approximation to the Navier–Stokes equations becomes

$$\begin{gathered} g'' + (\eta/2 + 1/\eta)g' + [(m+1)(m-2)/m](\beta - g) + [(m-1)/2]\eta\beta' \\ -[2(m-2)/m]w^2 = 0, \qquad g \equiv f + \eta f'/2, \end{gathered} \tag{68}$$

$$2(m-2)w^2 = m\eta\beta', \tag{69}$$

$$w'' + (\eta/2 + 1/\eta)w' - [\eta^{-2} + (m-2)/2m]w = 0. \tag{70}$$

These equations have to be solved with the matching boundary conditions as $\eta \to \infty$

$$f \to \eta^{2-4/m}, \quad \beta \to \eta^{2-4/m}, \quad w \to \eta^{1-2/m}, \tag{71}$$

and regularity conditions at the axis, $f \sim \eta^2$, $\beta \sim$ constant, and $w \sim \eta$. Equation (70) is decoupled from (68), (69), and its solution near the axis behaves as $w = A'\eta(1 - \eta^2/8m)$. Because the equation is linear, one may start the numerical integration by assigning an arbitrary value to A' and then rescaling the corresponding solution to match the behaviour found at infinity with that required by (71). Once w is known, f and β may be obtained by numerical integration of (68), (69), starting near the axis as $f = -B'[(m+1)(m-2)/8m]\eta^2$ and $\beta = B' + [(m-2)/m]A'^2\eta^2$, where B' is another free constant necessary to adjust the solution as $\eta \to \infty$ to (71). It should be noticed as a fundamental difference with the case $0 < m < 2$ that, owing to the linearity of equations (68) to (70), the regularization of the inviscid solution at the axis is always possible. Moreover, viscosity leaves unchanged the inviscid meridional velocity and pressure at the lowest significant order.

For $m < 0$, the scaling of the first-order terms of Ψ and p does not coincide with (66), (67) (see equations (26) and (28)), and the corresponding equations for f and β are different. However, (70) remains valid for $m < 0$ if one substitutes a_2 for a_1 in (65) to (70). Thus, the structure of the swirl inside the boundary layer, which is the only velocity component affected by viscosity at the lowest order, is the same in both cases $m < 0$ and $m > 2$.

4. Boundary layer at the cone surface for a negligible pressure gradient

The inviscid flow of section 2 is singular at the cone surface for $0 < m < 2$. By allowing for a thin boundary layer in the vicinity of $\theta = \alpha$, one can see that this singularity is associated with the action of a shear stress τ on the cone, where τ varies as a certain power of r. For a planar geometry, the pressure gradient is negligible along the boundary layer, and the fluid would be at rest far from the interface where the shear is imposed. Not so for a conical geometry, whose inviscid far field is, instead, that described in section 2. For $0 < m < 2$ it was shown that, even though the far field velocity does not vanish, the pressure gradient term is negligible compared to ρu_r^2 within the viscous region. In this section we will consider the general structure of this boundary layer, including also the possibility of a no-slip boundary condition on the cone surface. We shall see below that the pressure gradient is also negligible in comparison with the inertial terms when the inviscid flow is potential. This holds for any value of m, so the boundary layer analysis given in this section will also be valid for potential external flows.

Within the boundary layer approximation, we assume that the radial component of the velocity is much larger than the θ component, $u_r \gg u_\theta$, and that $\partial/\partial\theta \gg r\partial/\partial r$. Thus, the radial momentum equation in the narrow boundary layer near the cone surface $\theta = \alpha$ is

$$u_r \frac{\partial u_r}{\partial r} + \frac{u_\theta}{r}\frac{\partial u_r}{\partial \theta} = \frac{\nu}{r^2}\frac{\partial^2 u_r}{\partial \theta^2}, \tag{72}$$

where the pressure gradient term has been neglected. We have also neglected the terms containing the azimuthal velocity component because, as shown in section 2, $u_r \gg u_\phi$ in the boundary layer. The meridional motion inside the boundary layer is thus decoupled from the azimuthal velocity component, which is considered in Appendix C.†

† We are not considering here the case of an azimuthal motion induced by an azimuthal shear stress on the cone

Because the matching conditions (45) to (47) involve simple power laws and there are no external characteristic lengths, the problem admits solutions in terms of the similarity variable η:

$$\eta = \frac{\theta - \alpha}{\Delta(r)}, \tag{73}$$

where the combination of the standard condition $u_r \partial u_r/\partial r \sim \nu r^{-2}\partial^2 u_r/\partial\theta^2$ together with the definition of Ψ and (45) fix both the form of the stream function Ψ and the angular thickness of the boundary layer Δ as

$$\Psi = \frac{r\nu \sin\alpha}{\Delta} f(\eta), \tag{74}$$

$$\Delta^{m+2} = [(B\nu)^2(\sin\alpha)^{2-m}(m/KQ)^{2m}]r^{2(1-m)}. \tag{75}$$

The constants in $\Delta(r)$ have been chosen in such a way that the matching of (74) with the inviscid stream function (45) is automatically satisfied provided that $f(\eta) \to B(-\eta)^{m/2}$ as $\eta \to -\infty$, where B is an integration constant (see section 4.1.2 below). The velocity components are

$$u_r = \frac{\nu}{\Delta^2 r} f'(\eta), \quad u_\theta = -\frac{\nu}{(m+2)\Delta r}[3mf + 2(m-1)\eta f'], \tag{76}$$

where the primes denote differentiation with respect to η. Equation (72) becomes

$$f''' + \frac{3m}{m+2} ff'' + \frac{3(2-m)}{m+2} f'^2 = 0, \quad \eta < 0. \tag{77}$$

For potential flows, Ψ is still given by (74) in the boundary layer. However, according to (61), the angular thickness is now

$$\Delta = \frac{\nu f_\infty}{c \sin\alpha P'_{m'-1}(\cos\alpha)} r^{1-m'}, \tag{78}$$

where, as before, the constants in $\Delta(r)$ are such that $f(\eta) \to f_\infty$ as $\eta \to -\infty$, where f_∞ is an integration constant to be determined in section 4.1.3. In the above expression we have written m' instead of m to distinguish the two kinds of inviscid flows. If one makes the equivalence $m' = 3m/(m+2)$, the velocity components and the momentum equation are, for external potential flows, identical to (76), (77), so that the forthcoming analysis of (77) applies also to external potential flows by just changing the power m appearing in section 2.3 into $m' = 3m/(m+2)$.

Equation (77) is similar to the Blasius equation for the boundary layer of a uniform flow past a flat plate, being also invariant under two uniparametric groups of transformations:

$$\eta \to \eta + C_1; \quad f \to C_2 f, \quad \eta \to \eta/C_2, \tag{79}$$

where C_1 and C_2 are real arbitrary constants. Therefore, equation (77) can be reduced to the integration of a first-order differential equation followed by two quadratures, as discussed in

surface, in which case the meridional motion and the swirl may be coupled in the surface boundary layer (see Shtern and Hussain (**20**), where the case $m = 1$ is exhaustively analysed, including self-similar solutions with a non-vanishing azimuthal shear on the cone surface which couples the swirl and the meridional motion inside the surface boundary layer). The swirl, if it exists, is not induced by an azimuthal shear on the cone surface (see Appendix C, where only the cases with either $\tau_{\theta\phi} = 0$ or $u_\phi = 0$ at $\theta = \alpha$ are considered).

Bluman and Cole (**31**) for the Blasius problem. (Except for a change of scale in the variable η, the Blasius equation corresponds to the special case $m = 2$; actually $m' = 3/2$, since the external flow is potential for the Blasius problem.) This situation is unique in the sense that a two-dimensional phase plane picture describes completely all possible solutions to the problem for all values of the parameter m, and for all possible boundary conditions at the cone surface compatible with the self-similar variables used. An analysis of the phase plane structure is given in the next section, while in section 4.2 we will discuss some physically relevant boundary conditions.

4.1 *Phase plane analysis*

The two invariances (79) enjoyed by equation (77) suggest introducing new dependent and independent variables q and t which are invariant under the two groups of transformations (79):

$$q = \frac{1}{f^2}\frac{df}{d\eta}, \qquad t = f\,\frac{dq}{df}. \tag{80}$$

As a result, (77) becomes

$$-\frac{dt}{dq} = \frac{6q^2 + 7qt + t^2 + 3q + 3mt/(m+2)}{tq}. \tag{81}$$

The general form of the phase plane trajectories is sketched in Fig. 4 for some values of m, as follows from the following analysis of (81), which has four singular points:

$$(q,t) = (\infty,\infty), \quad (0,0), \quad [0, -3m/(m+2)] \quad \text{and} \quad (-\tfrac{1}{2}, 0). \tag{82}$$

Notice that when $m = 0$ the second and third singular points merge.

4.1.1 *Point $(q,t) = (\infty,\infty)$ or cone surface.* Only the quadratic terms on the right-hand side of (81) are relevant near this point. It is equivalent to $f''' = 0$, with behaviour

$$\eta \to 0: \quad f = c_1\eta + c_2\eta^2; \tag{83}$$

$$q = \frac{1}{c_1\eta^2}\left[1 - \frac{c_2^2\eta^2}{c_1^2} + \ldots\right]; \quad t = \frac{-2}{c_1\eta^2}\left[1 - \frac{c_2\eta}{c_1} + \ldots\right], \tag{84}$$

where c_1 and c_2 are constants. The point $(\eta, f) = (0,0)$ is thus at infinity in the (q,t)-plane, and is reached through the line $t = -2q$. There is one exceptional trajectory corresponding to the case $c_1 = 0$ of zero radial velocity on the cone surface, $f \sim \eta^2$, for which the point at infinity in (t,q)-space is reached along the path $t = -3q/2$. This special curve can be contructed numerically starting at infinity with $q > 0$ and $t = -3q/2$ and proceeding towards the origin, which attracts it automatically (see below). In the case $m = 2$, it corresponds to the solution to the Blasius problem and will be referred to as B or the Blasius separatrix (for all m).

4.1.2 *Point $(q,t) = (0,0)$ or inviscid vortical asymptote.* When $m \neq 0$, the origin can only be reached along the vertical axis or through the path

$$t = -\frac{m+2}{m}q\left[1 + q\left(\frac{4}{3m^2} - \frac{4}{m} - \frac{1}{3}\right) + \ldots\right], \tag{85}$$

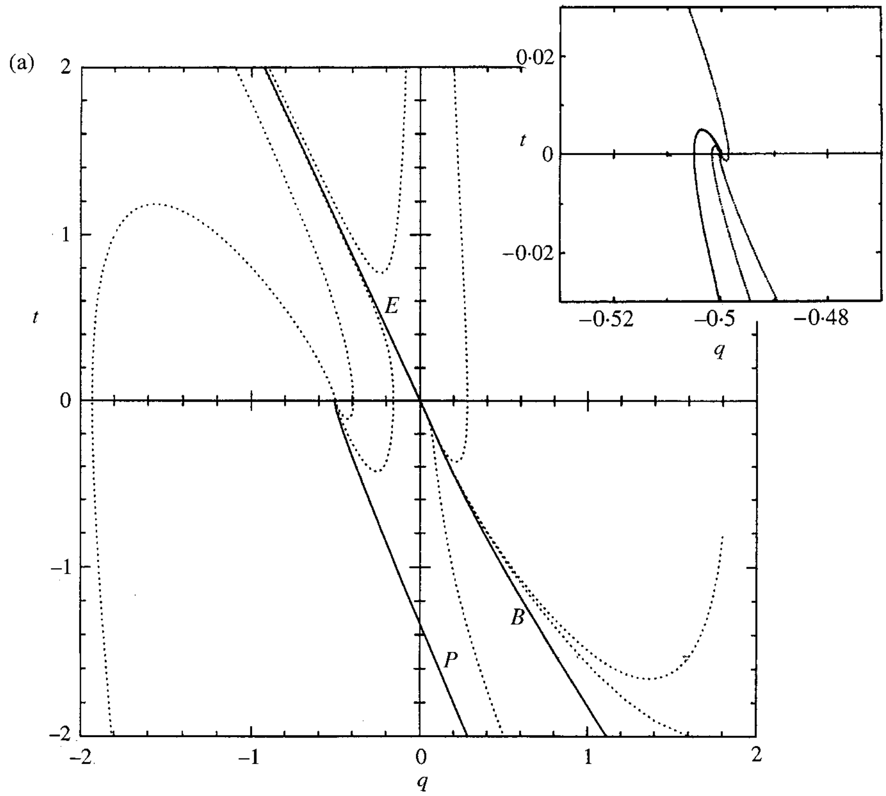

Fig. 4 (a) Phase plane structure (t vs q) for the boundary layer at the surface of the cone with negligible pressure gradient (81) for $m = \frac{8}{5}$ ($m' = \frac{24}{13}$). The vicinity of the singular point $(-\frac{1}{2}, 0)$ (which is a spiral for $m > 1{\cdot}07773$, and a node otherwise) is expanded

which corresponds to Euler's inviscid solution: $(2-m)f'^2+mff'' = 0$. This point is approached exponentially fast by all neighbouring trajectories as $q \to 0$ in the half-plane $q > 0$. The opposite behaviour (an exponential divergence of neighbouring trajectories as $q \to 0$) arises for $q < 0$. For $m > 0$, the upper half of the separatrix passing through the origin can be constructed numerically by starting the integration at the origin and moving towards $q < 0$. This upper curve will be subsequently referred to as E or as *Euler's separatrix.* The lower half of the curve coincides with the Blasius separatrix (see Fig. 4(a)). For $m < 0$, separatrix B disappears, while separatrix E is in the lower half of the plane, and it dies at the singular point $(q, t) = (0, -\frac{1}{2})$ (see Fig. 4(c)). At both sides of the origin, (85) may be written to lowest order in (η, f)-space as

$$f \to B(-\eta)^{m/2}, \tag{86}$$

where B is an arbitrary constant.

For $m = 0$, the third singular point (analysed below) merges with the origin, and the origin is only reached for $q < 0$ through the path (see Fig. 4(b))

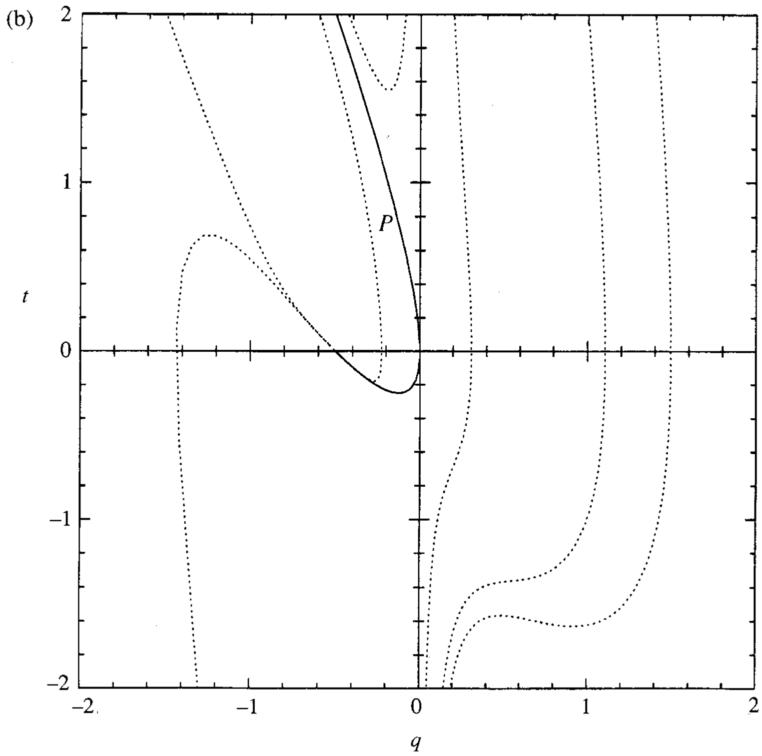

Fig. 4 (b) $m = m' = 0$

$$t = \pm\sqrt{(-2q)}. \tag{87}$$

All the neighbouring trajectories diverge from the origin as $q \to 0$. The exceptional trajectory reaching the origin for $t < 0$ (separatrix E) goes to the singular point $(q, t) = (0, -\frac{1}{2})$, while for $t > 0$ it reaches the singular point at infinity as $t = -2q$. In (η, f)-space, (87) corresponds to $\eta \to -\infty$ with f approaching a constant f_∞,

$$f \to f_\infty + \frac{2}{\eta}, \quad \eta \to -\infty, \tag{88}$$

very much as the solution associated with the trajectory reaching the singular point $(q, t) = [0, -3m/(m+2)]$ (which coincides with the origin for $m = 0$), analysed next. As we shall see, the solution associated with this exceptional trajectory asymptotes into a potential flow in the cone interior for any value of m. For $m = 0$, it can be expressed in closed form as the exact solution to (77)

$$f = \frac{f_\infty \eta}{\eta - 2/f_\infty}, \tag{89}$$

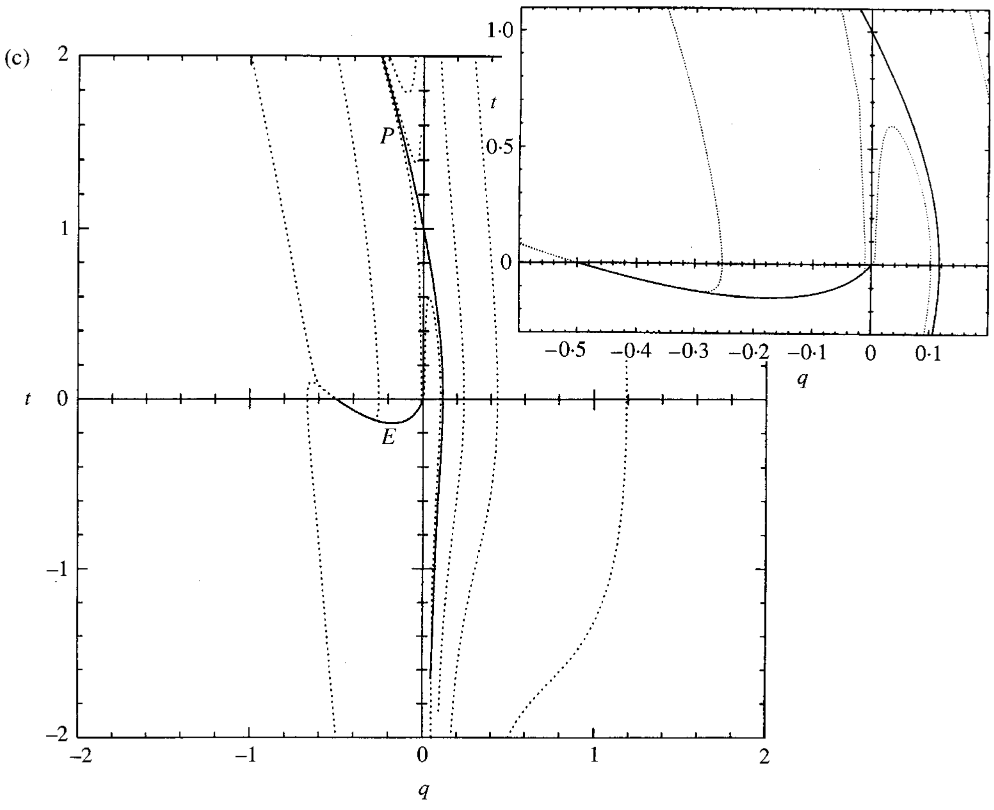

Fig. 4 (c) $m = \frac{1}{2}(m' = -1)$. The neighbourhood of the origin is expanded

earlier found by Mestel (**32**) in his surface boundary layer model for a Taylor cone.

4.1.3 *Point* $(q, t) = [0, -3m/(m+2)]$ *or potential cone interior.* Linearizing (81) in the vicinity of this point, for $m \neq 0$, one obtains

$$t = -\frac{3m}{m+2} - \frac{3m-1}{m}q + \frac{A}{s-s_0}, \quad q = -\frac{3m}{m+2}(s-s_0), \tag{90}$$

where A is an arbitrary constant. The point is an unstable saddle. For $m > 0$ this singular point lies in the lower half-plane, while for $m < 0$ it is in the upper half-plane. For $m = 0$ the point lies at the origin and was analysed above.

The exceptional path reaching this singular point (other than the vertical axis) can be constructed numerically by putting $A = 0$ in (90). For $m > 0$ ($m < 0$) the branch with $q < 0$ ($q > 0$) ends at the singular point $(q, t) = (-\frac{1}{2}, 0)$ (vertical axis), while that for $q > 0$ ($q < 0$) merges at $q \to +\infty$ ($q \to -\infty$) with the viscous solution $t \to -2q$, like all other neighbouring trajectories. This trajectory will be referred to as P, or the *potential separatrix,* because it corresponds to a viscous motion matching a potential flow in the core of the cone. In fact, in (η, f)-space, the singular point is reached as

$$f = f_\infty + C\ \exp[-3mf_\infty\eta/(m+2)] = f_\infty + C\ \exp[-m' f_\infty\eta], \quad \eta \to -\infty, \tag{91}$$

where f_∞ and C are arbitrary constants, $f_\infty < 0$ for $m' < 0$, and $f_\infty > 0$ for $m' > 0$, and, as shown in section 2.2, the asymptote $(\eta, f) \to (-\infty, f_\infty)$ corresponds to a potential flow in the interior of the cone. The motion represented by P is thus directed away from the apex for $m' > 0$, and towards the apex for $m' < 0$. Notice from (59) and (60) that p/ρ and u_r^2 are of the same order for potential flows as $x \to \alpha$. Yet, from (91), u_r decays exponentially to zero when approaching the inviscid asymptote. Because p/ρ remains constant across the boundary layer while u_r^2 increases dramatically, one has that $p/\rho \ll u_r^2$ inside the boundary layer. It is, accordingly, consistent to describe through (72) the boundary layer at the cone surface for an outer potential flow. The corresponding solution is that associated with P.

An interesting case arises at $m = m' = 1$, when P is given exactly by

$$t = -1 - 2q; \quad 1 + 2q = (f_\infty/f)^2; \quad f = f_\infty \tanh(f_\infty\eta/2) \qquad (m = 1). \tag{92}$$

This solution corresponds to the problem of a narrow two-dimensional jet (Schlichting's two-dimensional jet; see, for example, Schlichting (**33**)). However, the present jet is conical, and the coincidence is only in (η, f)-space, and not in physical variables. Because $f''(0) = 0$ in (92), this flow cannot represent a motion driven by shear at the cone surface, though this feature arises only for $m = 1$ (see 4.2.2).

4.1.4 *Point* $(q, t) = (-\frac{1}{2}, 0)$ *or Landau's singularity.* Linear analysis near this point shows that $q + \frac{1}{2} \sim t \sim e^{\lambda s}$, where λ solves the quadratic equation $\lambda^2 + (m+14)\lambda/(m+2) + 6 = 0$. Its real part is always negative for physically meaningful values of m, with real roots when $m \leq m* \simeq 1{\cdot}07773$, and imaginary roots otherwise. The point $(q, t) = (-\frac{1}{2}, 0)$ is therefore a stable spiral point for the case $m = 2$ (Blasius problem), and a stable node for $m = 1$ (Landau's axisymmetric jet and Schlichting's two-dimensional jet). The behaviour is $f = 2/(\eta - \eta_0)$ in (η, f)-space, and $\Psi = 2\nu r \sin\alpha/(\theta - \theta_0)$ in physical space, which, independently of the value of m, has the same r dependence as Landau's jet. Accordingly, we shall refer to the point $(q, t) = (-\frac{1}{2}, 0)$ as Landau's singularity. However, this singular point does not appear to be physically meaningful in the present problem, and we shall ignore all trajectories going through it.

4.2 *Description of the solutions*

From the above analysis one observes that all trajectories crossing or reaching the horizontal axis through a point different from the origin must be excluded because they exhibit a Landau-type singularity in physical variables. Therefore, for $m > 0$, only Euler's separatrix is a physically meaningful solution in the upper half-plane, while only those trajectories contained between the Blasius and the P paths (both included) are acceptable in the lower half-plane (see Fig. 4(a)). The upper half-plane solution (Euler path) with $q < 0$ corresponds to negative u_r, with the flow moving towards the cone tip. Trajectories in the lower half-plane represent the opposite behaviour. For $m \leq 0$, only separatrix P yields physically meaningful solutions for negligible pressure gradient, and it lies in the upper half-plane (see Figs 4(b) and 4(c)). Thus, for $m \leq 0$, the present solutions are only physically meaningful for an external potential flow, and m' should be used instead of m.

4.2.1 *Solutions compatible with a no-slip boundary condition on the cone surface.* The above analysis shows that only the Blasius path is compatible with a no-slip boundary condition on the cone surface [$c_1 = 0$ in (83)]. This trajectory behaves as $t = -3q/2$ as $(t, q) \to (-\infty, \infty)$, and goes towards the origin of the (t, q)-plane with behaviour (85), so it matches an inviscid vortical solution, which has physical meaning for negligible pressure gradient only when $0 < m < 2$ (in fact, Blasius's separatrix disappears for $m < 0$, see Figs 4(b) and 4(c)). However, since it lies in the lower half of the phase plane, it corresponds to a surface motion advancing away from the cone tip, which implies a near-axis inviscid motion directed towards the cone apex for one-cell flows. As shown in (**21**) (see section 3.1), these inviscid motions cannot be regularized at the axis.

In conclusion, the self-similar boundary layer equation considered in this section, which regularizes at the cone surface the present inviscid flows that are either potential for any value of m, or vortical ($K \neq 0$ or/and $K_1 \neq 0$) for $0 < m < 2$, cannot satisfy a no-slip boundary condition on the cone surface when these inviscid flows go out of the cone tip along the axis, and therefore can be regularized at the axis by a viscous layer. The above analysis includes the case $m = 1$, widely considered in the literature since it is the only case for which conically similar solutions to the full Navier–Stokes equations exist. The present result thus agrees with the known incompatibility of self-similar solutions for r^{-1} flows with a no-slip boundary condition, when this self-similar solution is allowed to be regular at the axis (see, for example, Sozou (**13**)). Of course, this does not mean that a non-self-similar solution may exist for the interaction of an r^{-1}-type vortex with a solid plane or cone. Actually, Burggraf *et al.* (**16**) found a numerical solution to the original boundary layer equations compatible with the no-slip condition which was not self-similar. For the present family of inviscid vortices with $0 < m < 2$, we have also found (**34**) that the original boundary layer equations have a numerical, non-self-similar solution satisfying the no-slip condition.

4.2.2 *Shear driven flows.* The present flows are compatible with a shear stress boundary condition of the form (3), that is,

$$\tau_{r\theta} = \frac{\mu}{r}\frac{\partial u_r}{\partial \theta} = j\Gamma_n r^n, \quad j = \pm 1, \quad \text{at} \quad \theta = \alpha, \tag{93}$$

where $j = +1$ corresponds to a shear stress pointing away from the cone tip, and $j = -1$ to a shear stress pointing towards the cone tip. As mentioned in the Introduction, the nearly inviscid flows generated by such a shear stress appear to be relevant to describe the motion sometimes observed inside Taylor cones. The relation between the powers n and m (or m' if the inviscid flow is potential) is obtained by substituting (76) into (93) and taking into account (75) (or (78) for potential flows):

$$n = \frac{2(2m-5)}{m+2} = 3m' - 5. \tag{94}$$

Since the present analysis is limited to $0 < m < 2$ for an inviscid vortical motion in the interior of the cone, only powers n in the range $-5 < n < -\frac{1}{2}$ are allowed in (93). In other words, the shear stress (93) produces a surface viscous motion with negligible pressure and matches an inviscid vortical flow only if n is between -5 and $-\frac{1}{2}$. Otherwise, the pressure gradient term is not negligible inside the surface boundary layer (see section 5). On the other hand, there is no *a priori* restriction on the values of n when the shear (93) induces a potential motion inside the cone (see, however, below).

The substitution of (75), (76) into (93) also yields the constant c_2 appearing in (83) ($f''(0) = 2c_2$) as a function of the shear constant Γ_n and other physical and numerical parameters. However, due to the second invariance (79), one may choose c_2 arbitrarily, for example, $c_2 = j/2$, because it will just change accordingly the scale of η through the constant B (or f_∞ for potential flows) appearing in the angular thickness Δ. Constants B and f_∞ in (86) and (91) are thus obtained numerically using the normalized boundary condition $f''(0) = j$. Once B and f_∞ are obtained (of course, they depend on m, and therefore on n), one has the following relations between the inviscid free constants K and c, and the shear constant Γ_n:

$$K = \frac{mB^{1/m}}{Q}\left(\frac{\Gamma_n}{\rho}\right)^{(m+2)/6m}\frac{(\sin\alpha)^{(2-m)/2m}}{\nu^{(m-1)/3m}}, \quad c = \left(\frac{\Gamma_n \nu}{\rho}\right)^{1/3}\frac{f_\infty}{\sin\alpha P'_{m'-1}(\cos\alpha)}. \tag{95}$$

From the second relation above it should be noticed that, given the cone angle α, the physical properties of the liquid, ρ and ν, and the shear stress (Γ_n and $n = 3m' - 5$), the constant c and, therefore, the potential flow in the interior of the cone, is uniquely fixed. However, this is not the case for inviscid vortical flows, for which K (the intensity of the swirl) is not fixed by those parameters because the constant $Q \equiv [2D/(2-m)]^{1/4}$ in (95) is not fixed. (Actually, since D is a combination of the inviscid parameters K and K_1, for a given K_1, K is not fixed by the shear stress, or, conversely, K_1 is not fixed for a given K.) This fact is related to the nature of the boundary layer equation for u_ϕ at the cone surface for a shear-driven flow (see Appendix C), where u_ϕ may be assigned arbitrarily without changing K. The constant K is thus determined during the initial unsteady set-up process, not considered here, as discussed by Shtern and Barrero (**35**, **36**) for the swirl appearance in liquid cones. Nevertheless, it was shown in (**21**) (see section 3.1) that for the present case $0 < m < 2$ the boundary layer at the axis fixes a limited range of values of D (and therefore of K through (95); that is, a limited range of K for a given K_1 through (21) and (95)) for which the solution can be regularized at the axis. Interestingly enough, for $0 < m < 1$, the allowed range of D excludes the possibility of swirl-less flows (see Fig.3), so the meridional motion produced by a *radial* shear stress like (93) has to be necessarily associated with an azimuthal motion. (This range includes the case $n = -\frac{5}{2}$ ($m = \frac{10}{13}$) of interest for the flow inside Taylor cones. Worth noticing is our experimental observation of the frequent appearance of swirl in these liquid cones.) For swirl-less non-potential flows ($K = 0$, $K_1 \neq 0$, which according to the results of section 3.1 are only possible for $1 < m < 2$), it is shown in Appendix C that K_1 is uniquely fixed by the matching condition at $\theta = \alpha$.

Figure 5(a) shows typical velocity profiles corresponding to a motion advancing towards the cone tip matching an inviscid vortical motion (path E), which from the above analysis can only represent a motion driven by a shear stress of the form (93) when $n < -\frac{1}{2}$. Figure 5(b) shows several velocity profiles for a motion matching a potential interior flow (path P). They are physically meaningful for $n \leq -5$ ($m' \leq 0$, corresponding to a flow directed away from the cone tip) and $n > -2$ ($m' > 1$, corresponding to a motion directed towards the cone tip). This is so because in the interval $-5 < n \leq -2$ ($0 < m' \leq 1$), f'' vanishes for some η, so that the velocity profiles go through an unphysical maximum (for $n = -2$ the maximum is on the cone surface, and the flow cannot be originated by a shear stress). In the range $-2 < n \leq -\frac{1}{2}$ ($1 < m' \leq \frac{3}{2}$), where the solutions are valid, f'' exhibits a maximum somewhere in the flow field, so that the radial velocity profile $f'(\eta)$ has an inflexion point, making the flow most likely unstable (except for $n = -\frac{1}{2}$ ($m' = \frac{3}{2}$), which is actually the Blasius solution).

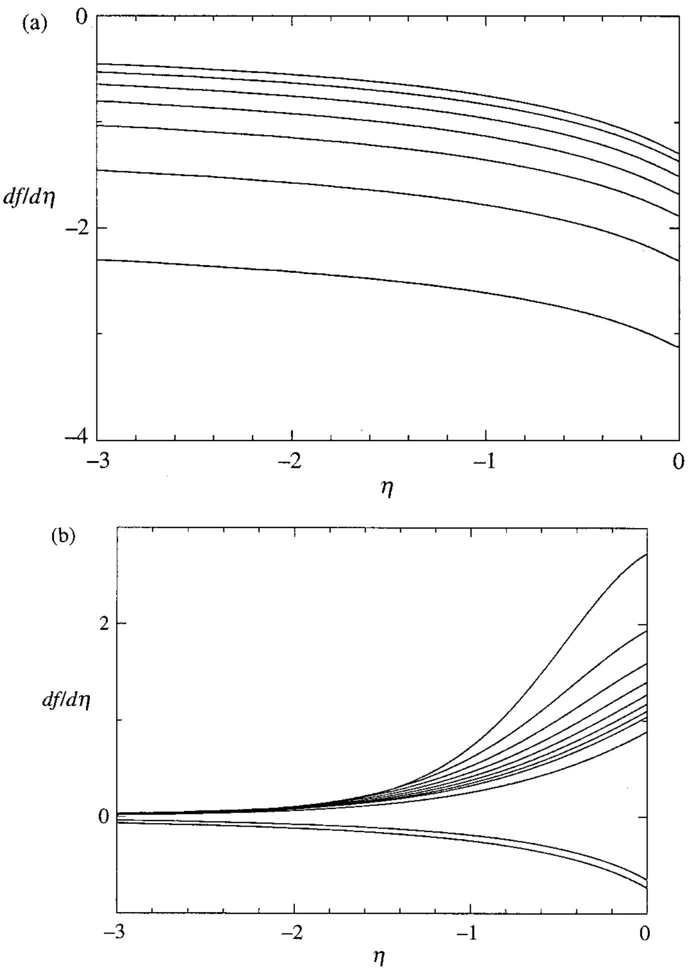

Fig. 5 Radial velocity profiles ($f'(\eta)$, equation (76)) in the boundary layer on the surface of the cone with negligible pressure gradient. (a) Motions corresponding to Euler's separatrix for, from top to bottom, $n = -2, -9/5, -8/5, -7/5, -6/5, -1$ and $-4/5$. All the curves are normalized to $f''(0) = -1$. (b) Motions corresponding to path P for, from top to bottom, $n = -7/4, -3/2, -5/4, -1, -3/4, -1/2, -1/4, 0, 1, -8$, and -6. The curves with $f'(\eta) > 0$ ($n > -5$) are normalized with $f''(0) = 1$, while those with $f'(\eta) < 0$ ($n \leq -5$) are normalized with $f''(0) = -1$

5. Boundary layer at the cone surface for non-negligible pressure gradient

When $m \leq 0$ or $m \geq 2$, the pressure gradient term $-(\partial p/\partial r)/\rho$ has to be added to the right-hand side of the radial momentum equation (72), where the terms containing the azimuthal velocity components are also negligible for these cases (the azimuthal momentum equation is analysed in Appendix C; see the footnote on p. 17). For $m < 0$ and $m > 2$ (the cases $m = 0$ and $m = 2$ are considered in Appendix A), the inviscid behaviours (29) to (31) and (53) to (55) allow for similarity solutions of that equation in terms of the variables

$$\eta = \frac{\theta - \alpha}{\Delta(r)}, \quad \Psi = \frac{r\nu \sin\alpha}{\Delta} f(\eta), \tag{96}$$

where

$$\Delta = \left(\nu/K^m\right)^{\frac{1}{2}} \; r^{(1-m)/2}. \tag{97}$$

(The case $K = 0$ is analysed in Appendix B.) The matching between inviscid and viscous flows implies that

$$f(\eta) \to \pm\gamma\eta \quad \text{as} \quad \eta \to \infty, \tag{98}$$

where $\gamma > 0$ is given by

$$\gamma = B_1 \quad \text{for} \quad m < 0, \text{ and} \quad \gamma = m^{1-m} G^{1/2} \quad \text{for} \quad m > 2, \tag{99}$$

and the $\pm$ signs account for motions directed towards, and away from, the cone tip. It is convenient, however, to use self-similar, non-negative, variables z and x into which the constant γ is absorbed:

$$f = -j \left(\frac{2j\gamma}{1+m}\right)^{1/2} z, \quad \eta = -\left(\frac{2j}{(1+m)\gamma}\right)^{1/2} x, \quad m \neq -1, \tag{100}$$

where $j = -1$ for $m < -1$ and $j = +1$ for $m > -1$ (see below). In these variables,

$$u_r = j\frac{\nu\gamma}{\Delta^2 r} z', \quad u_\theta = j\frac{\nu}{2r\Delta}\left(\frac{2j\gamma}{m+1}\right)^{1/2} [(1+m)z + (m-1)xz'], \tag{101}$$

where the primes mean derivatives with respect to x, and the momentum equation for $m \neq -1$, together with the matching boundary condition (98), transform into

$$z''' + zz'' + \frac{2(m-2)}{1+m}(1 - z'^2) = 0, \tag{102}$$

$$z'(\infty) = 1, \quad z(0) = 0, \tag{103}$$

where the condition that the cone surface is a streamline has also been added (the third boundary condition still needed to integrate (102) will be specified below). This is equivalent to the Falkner-Skan problem (see, for example, Jones and Watson (**37**)).

For $m = -1$ ($j = -1$ for this case; see below), one uses the variables

$$f = \surd(\gamma/3)\, z, \quad \eta = -x/\surd(3\gamma), \quad m = -1, \tag{104}$$

for which

$$u_r = -\frac{\nu\gamma}{\Delta^2 r} z', \quad u_\theta = \frac{\nu}{r\Delta}\sqrt{\frac{\gamma}{3}} x z', \tag{105}$$

and equation (102) transforms into

$$z''' + 1 - z'^2 = 0. \tag{106}$$

A solution of (106) with boundary conditions (103) in closed form was found by Pohlhausen (it corresponds to the flow in a converging channel; see, for example, Jones and Watson (**37**)):

$$z(x) = 3\surd 2[\tanh(x_0) - \tanh(x_0 + x/\surd 2)] + x, \quad m = -1, \tag{107}$$

where x_0 will be fixed by the still unspecified third boundary condition (see below).

To solve (102) numerically we reduce its order by using the variable

$$g = 1 - z'^2, \tag{108}$$

through which it becomes

$$(1-g)^{\frac{1}{2}} \frac{d^2 g}{dz^2} + z\frac{dg}{dz} - \frac{4(m-2)}{1+m} g = 0, \quad m \neq -1, \tag{109}$$

$$g \to 0 \quad \text{as} \quad z \to \infty. \tag{110}$$

The behaviour of the solution as $z \to \infty$ ($x \to \infty$) is

$$g \to k_1 z^{4(m-2)/(1+m)} + k_2 z^{(7-5m)/(1+m)} e^{-z^2/2}, \quad z \to \infty, \quad m \neq -1, \tag{111}$$

where k_1 and k_2 are arbitrary constants. For $m \leq -1$ and $m \geq 2$, the condition $g \to 0$ as $z \to \infty$ implies that the first term in (111) must vanish ($k_1 = 0$; notice that this term is the dominant one when the pressure gradient is negligible—compare with equation (86)). Also, from the above equations, the only allowed motion when $m \leq -1$ is one directed towards the cone tip ($j = -1$), while for $m > 2$ only a motion directed away from the cone tip is possible ($j = +1$). For $-1 < m < 0$, the constant k_1 may be different from zero. However, the solutions for these values of m are not physically meaningful because they present a maximum in the velocity profile. (The situation is similar to that found in section 4.2.2 for solutions corresponding to path P for $-5 < n < -2$.) These unphysical solutions with *supervelocities* are typical of the Falkner-Skan problem when the constants multiplying the second and third terms in (102) have opposite signs (Stewartson (**38**)), that is, when $-1 < m < 2$ in our problem (note that for $0 < m < 2$ the present solutions are not valid because the pressure gradient term is negligible, that is, $\gamma \simeq 0$).

The numerical integration of (109) is started from the exceptional path corresponding to $k_1 = 0$ of the point at infinity, which is a node for both $m < -1$ and $m > 2$. The integration proceeds, in (g, z) variables, until the cone surface $z = 0$ is reached (this point is also a node). Constant k_2 is selected in such a way that a third boundary condition, not yet specified, is satisfied. As in section 4, we shall consider two different boundary conditions on the cone surface: a no-slip boundary condition ($z'(0) = 0$), and a shear stress boundary condition compatible with the self-similar structure ($z''(0) = \text{constant}$). In both cases, the numerical value of k_2 is selected by shooting until one of these two boundary conditions on the cone surface is met. Once the function $g(z)$ is known, $z(x)$ is obtained from the quadrature

$$dz/dx = j[1 - g(z)]^{1/2}, \tag{112}$$

where the starting value for x may be chosen arbitrarily due to the invariance of the equations under any shift of x (the origin of x is selected such that $z(x = 0) = 0$).

5.1 *Solutions compatible with a no-slip boundary condition*

If the additional condition of zero velocity on the cone surface,

$$z'(0) = 0, \tag{113}$$

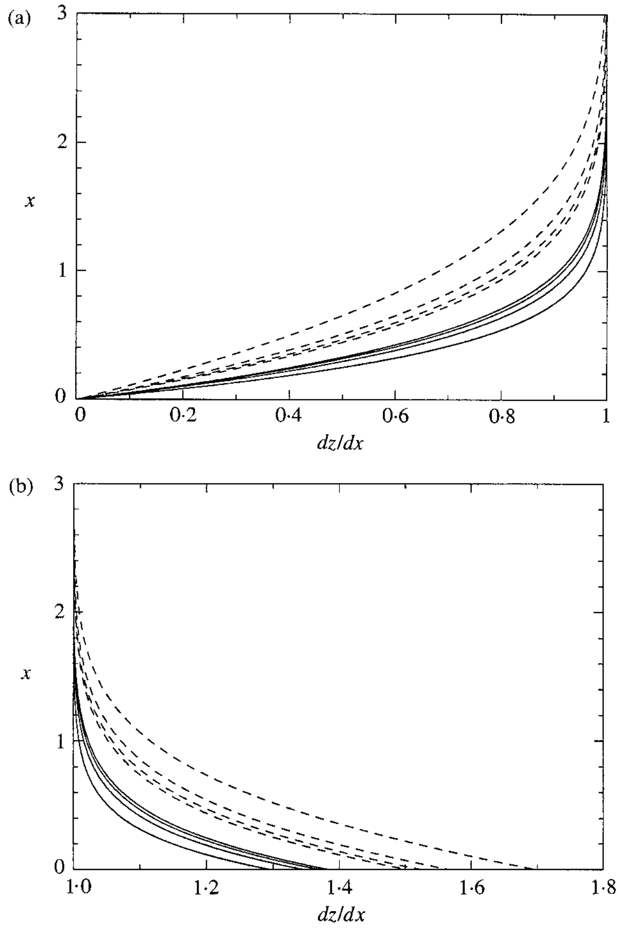

Fig. 6 Radial velocity profiles ($z'(x)$, equation (101)) in the boundary layer at the cone surface with non-negligible pressure gradient term. (a) Motions with $u_r = 0$ on the cone surface ($z'(0) = 0$) for some values of m. Dashed lines are for, from top to bottom, $m = 3, 5, 7$ and 9; solid lines are for, from bottom to top, $m = -3, -5, -7$ and -9. (b) The same as in (a), but for a given shear stress on the cone surface. The curves are normalized with $z''(0) = -1$

is imposed on (102) (or (106)), one recovers exactly the Falkner–Skan problem. However, because the present problem has conical rather than planar symmetry, this identity is only in the self-similar variables, and not in the physical variables.

For $m = -1$, (113) fixes $x_0 = \tanh^{-1}\sqrt{\frac{2}{3}}$ in (107). However, it is shown in Appendix C that for $m = -1$ the azimuthal velocity in the boundary layer cannot match the external inviscid behaviour, for any boundary condition on the cone surface. Yet, the above solution is valid for swirl-less flows ($K = 0$, see Appendix B). Thus, solutions with a no-slip boundary condition are possible for $m < -1$ and $m > 2$ (also for $m = -1$ in the case of swirl-less flows). For $m < -1$

(and $m = -1$ if $K = 0$), only a surface flow directed towards the cone tip is possible, while for $m > 2$, only the opposite direction is allowed. Figure 6(a) shows numerical solutions for $z'(x)$ for some values of m.

5.2 *Shear-driven flows*

The self-similar flows under consideration are also compatible with a shear stress boundary condition of the form (93) ($z''(0) = $ constant) for some ranges of values of n. In fact, substituting u_r from (101) (or (105)) into (93), the following relation between the powers n and m is obtained:

$$n = \tfrac{1}{2}(3m - 7), \quad m \le -1 \quad \text{or} \quad m > 2. \tag{114}$$

Since we have shown above that the present solutions are valid for $m \le -1$ and $m > 2$, the allowed values of n are $n \le -5$ and $n > -\frac{1}{2}$, thus complementing the range $-5 < n < -\frac{1}{2}$ considered in section 4.2.2, for which the pressure gradient term is negligible inside the viscous boundary layer at the cone surface. Also, from the above analysis, a shear stress with $n \le -5$ is only possible when it points towards the cone tip ($j = -1$), and a shear stress with $n > -\frac{1}{2}$ is only possible when it is directed away from the cone apex.

To integrate numerically (102) by the procedure described above, we fix

$$z''(0) = -1. \tag{115}$$

Numerical solutions for $z'(x)$ thus normalized are given in Fig. 6(b) for some values of $m \le -1$ and $m > 2$. (The solution for $m = -1$ is given by (107), where the condition $z''(0) = -1$ fixes x_0 as $\tanh(x_0)/\cosh^2(x_0) = -\sqrt{2}/6$; however, as discussed above, this solution is only valid for swirl-less flows, $K = 0$.) With this normalization, the following relation between the parameters of the problem is obtained for $m \neq -1$:

$$K^m = \frac{1}{\gamma}\left(\frac{2j\Gamma_n^2}{(1+m)\nu\rho^2}\right)^{1/3}, \quad m \neq -1 \quad (n \neq -5). \tag{116}$$

This relation fixes the intensity of the swirl K for a given shear stress (Γ_n and m), a given liquid (ρ and ν), and given γ, which is related to the inviscid constants B_1 ($m \le -1$) or G ($m > 2$) (see (99)). These last constants are functions of m, the cone angle α, and the inviscid parameter D (see section 2). The situation is thus similar to that found for vortical inviscid flows with $0 < m < 2$ discussed in section 4.2.2: since D is a free parameter, and it relates the intensity of the swirl K with that of the inviscid meridional motion K_1, the shear stress, together with the other physical parameters, fix the intensity of the meridional motion, but not the swirl intensity, which is determined during the steady set-up process. The only physically important difference with the case $0 < m < 2$ analysed in section 4.2.2 is that, for that case, the boundary layer at the axis forbids some ranges of D, which sometimes excludes the possibility of swirl-less motion, while for $m \le -1$ and $m > 2$, there is no limitation on D and, therefore, on K. The case $K = 0$ is considered in Appendix B, where it is shown that, obviously, the intensity of the inviscid meridional motion K_1 is fixed by the shear stress, for a given liquid and cone angle.

For $m = -1$, only the case $K = 0$ is possible, and the relation between the intensity of the meridional motion and the shear stress parameters is given in Appendix B.

6. Summary and discussion of one-cell solutions

The family of one-cell flows analysed so far generalizes, for high Reynolds numbers, the known class of conical swirling flows with velocity field varying as r^{-1} (case $m = 1$), which constitutes the only instance for which the full Navier–Stokes equations have conically similar solutions (see, for example, the references cited in the Introduction). Squire (**6**) and Goldshtik (**7**) showed that these solutions, if they are regular at the axis, are incompatible with the condition of zero velocity on a cone surface for Reynolds numbers above a critical value (see also Yih *et al.* (**8**), and Sozou (**13**), among others). A similar result was found for the interaction of a potential vortex ($u_\phi \sim r^{-1}$) with a cone or a plane, first considered by Taylor (**14**). Burggraf *et al.* (**16**), among others, showed that no self-similar solutions existed for the boundary layer induced by a potential vortex on a plane wall, though these authors were able to find a two-layer structure for that boundary layer. This work was later extended by the same authors (Belcher *et al.* (**24**)) to the interaction of a *generalized* vortex of the form $u_\phi \sim r^{-n}$ with a plane. They found *numerically* that self-similar solutions for the boundary layer may exist only for $n < n_0$, where $n_0 \simeq 0{\cdot}1217$. Though the inviscid vortices considered by these authors are not exactly equivalent to our conical inviscid vortices, which are *exact* solutions to Euler's equations, our results agree with those by Belcher *et al.* (**24**) in that the non-existence of similarity solutions for the r^{-1} case is not unique. Thus we find *analytically* that no self-similar solutions exist for the boundary layer induced by an inviscid conical vortex on a conical wall (or a plane) when $-1 \leq m \leq 2$, which includes the case $m = 1$. The same result is also found for potential flows for any value of m (recall that the only case for which a potential flow may have non-zero azimuthal velocity is $m = 1$, which corresponds to the potential vortex considered by Burggraf *et al.* (**16**); see section 2.2). For $m < -1$, we find that self-similar solutions compatible with a no-slip boundary condition on a cone surface are possible only when the near-surface flow is directed towards the origin, while, for $m > 2$, only the opposite direction is allowed (see Fig. 7). (For $m = -1$, the inviscid motion is compatible with a no-slip boundary condition when it is swirl-less, $K = 0$, but non-potential, $K_1 \neq 0$.)

In addition to the important physical problem of the interaction of a conical nearly inviscid vortex with a conical wall or a plane, which is of interest for modelling atmospheric vortices or the flow in vortex chambers, we have considered the case of nearly inviscid conical flows driven by a shear stress of the form (3), which appears to be related to the shear-driven flow inside Taylor cones. Figure 8 sketches all the possible steady flows as a function of n and j: Fig. 8(a) shows the regions of existence of solutions corresponding to vortical inviscid motions in the interior of the cone, and Fig. 8(b) shows those corresponding to potential flows in the cone core. The upper parts of the figures represent flows with $j = +1$, which corresponds to a shear stress pointing away from the cone tip, and the lower parts are for $j = -1$, corresponding to a shear stress pointing towards the cone tip. Relevant values of n for existence of solutions, along with the corresponding values of m, are represented in the horizontal axis: in Fig. 8(a) the relation $m(n)$ is given by (94) or by (114), corresponding to inviscid vortical flows with negligible and non-negligible pressure inside the surface boundary layer ($\gamma = 0$ and $\gamma \neq 0$) respectively; in Fig. 8(b), the relation $m'(n)$ is given by (94).

Beginning with solutions corresponding to inviscid vortical flows in the interior of the cone (Fig. 8(a)), when $n \leq -5$, they are possible only with $j = -1$, and are such that the pressure gradient is not negligible at the cone surface ($\gamma \neq 0$), so that this interval is equivalent to $m \leq -1$. For $n > -\frac{1}{2}$, solutions exist only for $j = +1$ and $\gamma \neq 0$ ($m > 2$). For $-5 < n \leq -\frac{7}{2}$

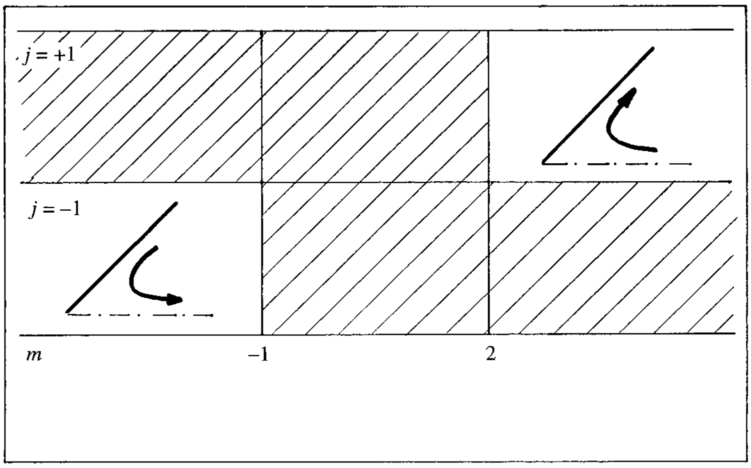

Fig. 7 Sketch of the regions of existence of solutions in the (m, j) parameter space of steady conical flows at high Reynolds numbers compatible with null velocity on the cone surface. The upper part of the figure is for flows with near-surface motion directed away from the cone tip ($j = +1$). The lower part is for flows directed in the opposite direction ($j = -1$). No solutions exist in the shaded areas

and $j = \pm 1$, the boundary layer at the cone surface with $\gamma \neq 0$ $(-1 < m \leq 0)$ are not physically meaningful because they present supervelocities; in this range of values of n, γ might also be equal to zero $(0 < m \leq \frac{2}{5})$, and solutions only exist for $j = -1$, since the inviscid flow for $j = +1$ cannot be regularized at the axis. The same situation occurs for $-\frac{7}{2} < n \leq -\frac{1}{2}$ (in this interval $\gamma = 0$, so that it corresponds to $\frac{2}{5} < m \leq 2$): the inviscid flow may be regularized at the axis only for $j = -1$. However, this regularizing boundary layer at the axis imposes some restrictions on the permissible values of the ratio between swirl and the meridional motion intensities in the inviscid flow (parameter D or swirl parameter L; see Fig. 3). Finally, for $n = -\frac{1}{2}$, the inviscid solution (for which $\gamma \neq 0$, and the boundary layer at the cone surface allows only $j = +1$) cannot be regularized at the axis.

In relation to solutions corresponding to potential flows in the core of the cone (Fig. 8(b)), they are regular at the axis, so that no viscous layer is needed there, and are regularized at the cone surface by solutions to the boundary layer equations with $\gamma = 0$ passing through path P. For $n > -5$ $(m' > 0)$, only solutions with $j = +1$ are possible, while for $n \leq -5$ $(m' \leq 0)$, solutions are only possible for $j = -1$. However, in the interval $-5 < n < -2$ $(0 < m' < 1)$, the boundary layer at the cone surface yields supervelocity solutions, which are not physically meaningful.

It is observed that a shear stress of the form (3) pointing away from the cone tip ($j = +1$) with a power n between -2 and $-\frac{1}{2}$ is compatible only with a potential, steady flow in the cone core, while a shear stress pointing towards the cone tip ($j = -1$) with $-5 < n < -\frac{1}{2}$ is compatible only with an inviscid vortical, steady motion in the interior of the cone. Within this range, when $-5 < n \leq -2$ $(0 < m \leq 1)$, steady solutions exist only for swirling flows ($K \neq 0$), while for $-2 < n < -\frac{1}{2}$ $(1 < m < 2)$, flows with both $K = 0$ (but with $K_1 \neq 0$, that is, the flow

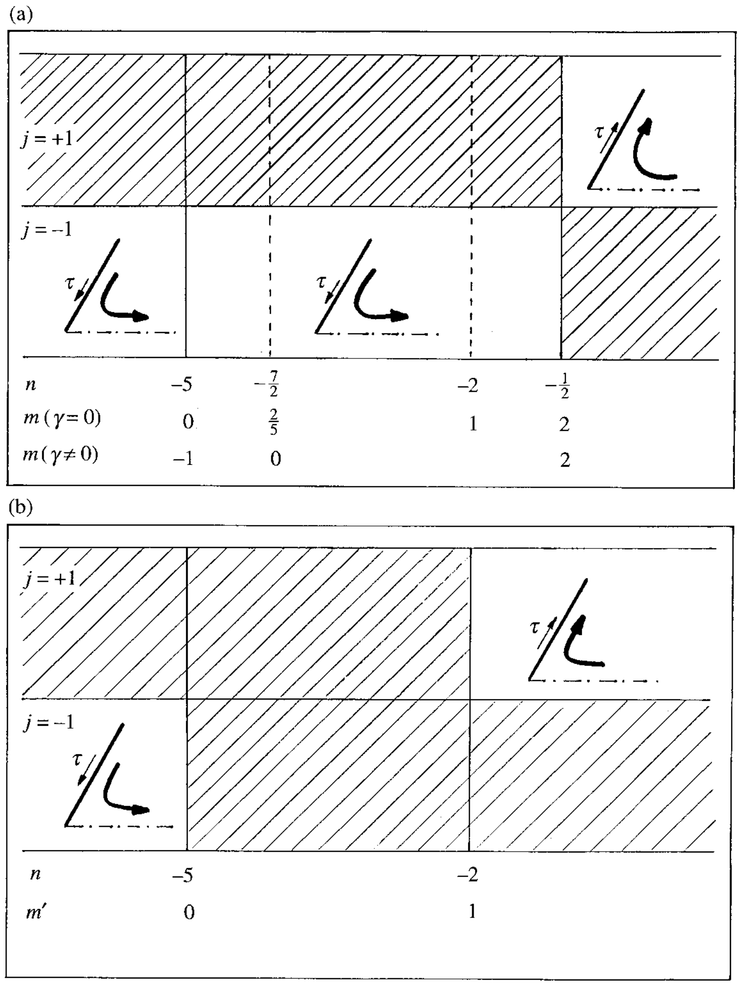

Fig. 8 Sketch of the regions of existence of solutions in the (n, j) parameter space of steady conical flows at high Reynolds numbers driven by a surface shear stress of the form (3) corresponding to inviscid vortical flows (a) and potential flows (b) in the interior of the cone. The upper parts of the figures are for flows with $j = +1$, and the lower parts for $j = -1$. No solutions exist in the shaded areas

cannot be potential) and $K \neq 0$ are possible. When $n > -\frac{1}{2}$ (in this interval, solutions are only possible when the shear stress points away from the cone tip, $j = +1$) and $n \leq -5$ (solutions are possible only for $j = -1$), the inviscid steady motion may be rotational or irrotational, depending, possibly, on the unsteady set-up process and the asymmetries of the incoming flow (Shtern and Barrero (**34**, **35**)). Finally, for $n \leq -2$ with $j = +1$, and for $n \geq -\frac{1}{2}$ with $j = -1$, no steady solutions at high Reynolds numbers exist.

Notice that, in addition to the physical applications already mentioned, the one-cell solutions given above may be of interest in other problems. In particular, this analysis enriches further our present knowledge of boundary layers for inviscid rotational flows with several new and fairly simple examples. Thus, for instance, we present new cases for which a boundary layer with self-similar structure, both near a conical surface or a plane, and near the axis of symmetry, ceases to have a solution. In the case of near-axis swirling flows, we show in (**21**) that this property of solution breakdown supports, with a clear example, one of the existing theories (Hall (**18**)) on vortex breakdown. The two-cell structure of the flow when one-cell solutions break down (for $0 < m < 2$) is analysed next.

7. Two-cell inviscid flow

At high Reynolds numbers, the structure of a two-cell conical flow consists of a slender viscous conical fan-jet separating two inviscid regions (see, for example, Shtern and Hussain (**19**) for the case $m = 1$, and the sketch in Fig.1(b)). In order for the inner inviscid cell to be regular at the axis, the flow must be potential (see section 7.2 below). Thus we shall use the results of section 2.2 between $\theta = 0$ and a certain conical surface $\theta = \theta_s$, $0 < \theta_s < \alpha$. At $\theta = \theta_s$ one has a fan-jet layer matching the inner and outer inviscid cells. The meridional motion in this interior layer is described by the same equation analysed in section 4. Finally, the outer cell between $\theta = \theta_s$ and $\theta = \alpha$ has to be vortical because of the matching with the fan-jet layer. We first analyse in this section the two inviscid cells.

Mathematically, for the outer cell one has to solve (16) with the boundary conditions $F(\theta_s) = F(\alpha) = 0$.† For the inner potential cell the boundary conditions are $F(0) = 0$, $F(\theta_s) =$ constant. Both θ_s and the constant are obtained from the matching.

7.1 *Outer inviscid vortical cell*

Let us look for a solution of (16), in the domain $\theta_s < \theta < \alpha$, satisfying the boundary conditions $F(\theta_s) = F(\alpha) = 0$. The fan-jet position θ_s is unknown and must be obtained as part of the solution.

Following the analysis performed in section 2.1.2 describing the solutions of equation (34) near $\theta \to \alpha$, the behaviour near $\theta \to \theta_s$ ($x \to x_s = \cos\theta_s$) can be seen to be the following (equation (41)):

$$y = I(x_s - x)\left[1 + \frac{2G}{3-m} I^{-m}(x_s - x)^{2-m}\right] - \frac{(x_s - x)^2}{1 - x_s^2} - \frac{2(m-1)}{3m(1-x_s^2)}\left(I - \frac{2x_s}{1-x_s^2}\right)(x_s - x)^3 + \ldots, \tag{117}$$

where $I \equiv (2D/(2-m))^{\frac{1}{2}}$. The corresponding behaviours of the stream function, velocity and pressure fields as $x \to x_s$ are

$$\Psi = r^m A^{m/4}(x_s - x)^{m/2}, \quad u_r = (m/2) r^{m-2} A^{m/4}(x_s - x)^{(m-2)/2},$$
$$u_\theta = -r^{m-2}\frac{m A^{m/4}}{\sin\theta_s}(x_s - x)^{(m-2)/2}, \tag{118}$$

$$u_\phi = K r^{m-2} A^{(m-1)/4}(1 - x_s^2)^{-1/2}(x_s - x)^{(m-1)/2}, \tag{119}$$

$$p/\rho = K^{2m} r^{2(m-2)}\left[-m^{2(1-m)}G/2 - \frac{I^{m-1}}{2m^{2m-1}(1-x_s^2)}\left(I - \frac{2x_s}{1-x_s^2}\right)(x_s - x)^m\right], \tag{120}$$

† Except for $m = 1$, for which $F(\theta_s) =$ constant (see the end of section 8).

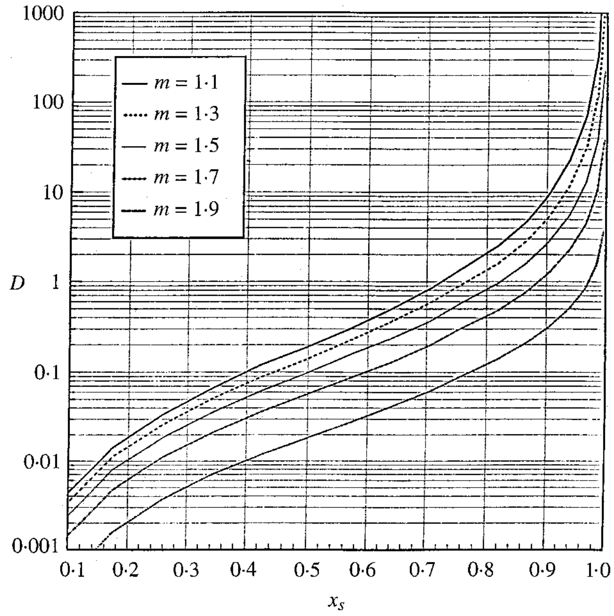

Fig. 9 Values of D as a function of the jet-fan position x_s for $\alpha = \pi/2$ and several values of m

where, for simplicity, we have defined

$$A \equiv \frac{2DK^4}{m^4(2-m)} = I^2(K/m)^4. \tag{121}$$

The constant G in (120) must be obtained by matching the outer and the inner cells through the fan-jet layer solution. The corresponding analysis will be carried out in the next section to show that $G = 0$. This condition determines the position θ_s of the fan-jet as a function of m, D, and the cone angle α. To obtain $\theta_s(\alpha, D, m)$ numerically, it is convenient to start the integration of (34) at a fixed value of x_s, using the behaviour (117) with $G = 0$, and sweeping in D until finding the value of α for which $y(\cos\alpha) = 0$. Figure 9 shows D as a function of $x_s \equiv \cos\theta_s$ for $\alpha = \pi/2$ and several values of m ($1 < m < 2$). The dimensionless stream function $(m/Kr)^m\Psi(x)$ in the outer cell ($\cos\alpha > x > \cos\theta_s$) is plotted in Fig. 10 for $\alpha = \pi/2$, $m = 1{\cdot}6$ and $\theta_s = \pi/3$.

7.2 *Inner potential flow*

For $0 < m < 2$, the flow in the inner cell must be potential since according to (**21**) (see also section 3.1) no inviscid vortical flow with downward axial velocity can be regularized at the axis; that is, $K = K_1 = 0$. As shown in section 2.2, the stream function Ψ is related to the Legendre functions $P_{m'-1}$ by

$$\Psi = cr^{m'}(1-x^2)P'_{m'-1}(x), \tag{122}$$

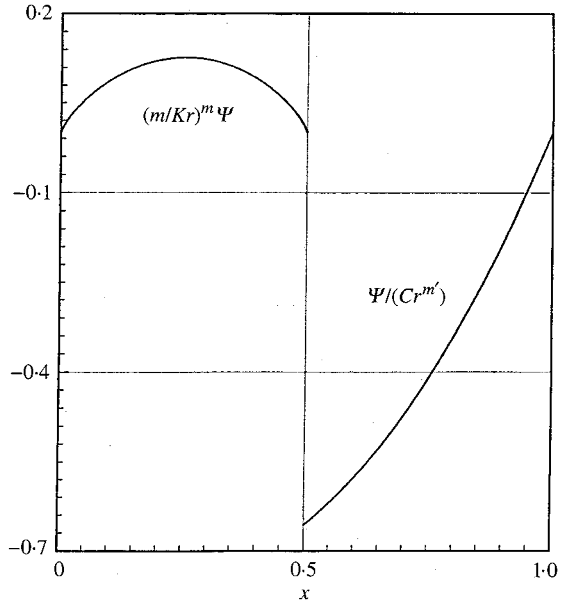

Fig. 10 Dimensionless stream function in the outer and the inner cells for $\alpha = \pi/2, \theta_s = \pi/3$ and $m = 1{\cdot}6$

where c is a constant which, together with m', will be determined from the matching with the fan-jet solution as $x \to \cos\theta_s$. Note from (122) that the existence of solutions of the two-cell type is restricted to non-negative values of the index of the Legendre functions, that is, $m' \geq 1$.

Along with (122), the fluid variables are given by (59)–(60) with m replaced by m'. The dimensionless stream function $\Psi(x)/(cr^{m'})$ in the inner cell, $\cos\theta_s < x < 1$, is plotted in Fig. 10 for $\alpha = \pi/2$, $m' = 4/3$ (which as shown below corresponds to $m = 1.6$) and $\theta_s = \pi/3$. The jump that Ψ presents at $\theta = \theta_s$ indicates that there exists an inner viscous layer corresponding to a jet flowing out along the cone $\theta = \theta_s$.

8. Fan-jet viscous layer

The stream function at x_s needs to be regularized through a viscous boundary layer whose angular thickness Δ, determined by the standard condition $u_r \partial u_r/\partial r \sim (\nu/r^2)\partial u_r/\partial\theta$, is inversely proportional to the square root of the Reynolds number

$$\Delta \sim \left[\frac{\nu}{r u_r}\right]^{1/2}, \tag{123}$$

or, taking into account (118),

$$\Delta \sim \left[\frac{\nu}{r^{m-1} A^{m/4}}\right]^{2/(m+2)}, \tag{124}$$

which is assumed small. Since $0 < m < 2$, equations (118) to (120) show that $u_r \to \infty$, $u_\theta \to 0$, $u_\phi \ll u_r$ and $p/\rho \ll u_r^2$ as the flow approaches the fan-jet surface from the outer cell. Accordingly, the pressure gradient term and the terms containing the azimuthal velocity component may be neglected in the radial momentum equation, as in (72). Therefore, the meridional motion is decoupled from the swirl inside the fan-jet layer, and one may use the analysis given in section 4 to describe this meridional motion, by using appropriate matching conditions with both the outer and inner cells. Once the meridional motion is known, the azimuthal velocity component is described by a linear equation, as in Appendix C for the swirl in the surface boundary layer. This azimuthal motion inside the fan-jet layer is considered in Appendix D together with the corresponding pressure field.

Although all the possible self-similar meridional motions governed by (72) (together with the continuity equation, of course) were exhaustively analysed in section 4 in connection with the boundary layer at $\theta = \alpha$, it is convenient to reproduce part of those results here in order to adapt them to the fan-jet boundary layer. Defining the following self-similar variables:

$$\Psi = A_1 r^{3m/(m+2)} f(\eta), \tag{125}$$

$$\eta = \frac{\theta - \theta_s}{\Delta(r)}, \quad \Delta(r) = A_2 r^{2(1-m)/(m+2)}, \tag{126}$$

where

$$A_1 = \left[A\nu^2(1 - x_s^2)\right]^{m/2(m+2)}, \quad A_2 = \left[\nu(1 - x_s^2)^{(2-m)/4} A^{-m/4}\right]^{2/(m+2)}, \tag{127}$$

the radial and meridional velocity components can be expressed as

$$u_r = \frac{1}{r^2(1 - x_s^2)^{1/2}} \frac{\partial \Psi}{\partial \theta} = \frac{A_1 r^{3(m-2)/(m+2)}}{A_2(1 - x_s^2)^{1/2}} f'(\eta), \tag{128}$$

$$u_\theta = -\frac{1}{r(1 - x_s^2)^{1/2}} \frac{\partial \Psi}{\partial r} = -\frac{A_1 r^{(m-4)/(m+2)}}{(m+2)(1 - x_s^2)^{1/2}} [3mf - 2(1-m)\eta f'(\eta)], \tag{129}$$

and the radial momentum equation (72) results in the ordinary differential equation (77), but now η may be both positive or negative.

The inviscid stream functions of both outer and inner solutions behave when $\theta \to \theta_s$ as (see (118) and (122)):

$$\Psi^{\text{outer}}_{\theta-\theta_s\to 0} \to [A(1 - x_s^2)]^{m/4} r^m (\theta - \theta_s)^{m/2} = [A(1 - x_s^2)]^{m/4} r^m \eta^{m/2} \tag{130}$$

and

$$\Psi^{\text{inner}}_{\theta_s-\theta\to 0} \to -cr^{m'}(1 - x_s^2) P'_{m'-1}(x_s). \tag{131}$$

Thus, matching (130) and (131) with (125) requires

$$m' = \frac{3m}{m+2}, \tag{132}$$

$$f(\eta \to \infty) \to \eta^{m/2}, \tag{133}$$

$$f(\eta \to -\infty) \to f_{-\infty} = -c(\nu^2 A)^{-m/(2m+4)} (1 - x_s^2)^{2/(m+2)} P'_{m'-1}(x_s). \tag{134}$$

Conditions (133) and (134) must be used as boundary conditions for (77). Since m' must be larger than or equal to unity, equation (132) shows that the existence of two-cell type flows is restricted to values of m within the interval $1 \le m < 2$. This is not surprising because only in this range does solution breakdown of the near-axis boundary layer equations occur *above* a threshold value of the swirl parameter (see section 3.1), as observed in vortex breakdown.

In terms of the phase plane variables (q, t) of section 4.1, behaviours (133) and (134) correspond to the singular points $[0, 0]$ and $[0, -3m/(m+2)] = [0, -m']$, respectively, of the phase plane, and the solutions described below coincide with the P path and the trajectories lying between that path and the Blasius path (see Fig.4). In particular, the relevant solution starts at the singular point $[0, -3m/(m+2)]$, corresponding to the potential flow end, goes towards $(q, t) = (\infty, -\infty)$ as $t = -2q$, and then goes backwards towards the origin, corresponding to the rotational inviscid end. Here, we will give some details of the numerical integration of (77) in the present case, which are also useful to simplify the analysis of Appendix D. First, on using the invariance of (77) under the second of the transformations (79), we define

$$\zeta = R\eta, \quad \varphi = f/R, \tag{135}$$

where R is an arbitrary constant, which, for convenience, will be chosen as

$$R = -\frac{3m}{m+2} f_{-\infty}. \tag{136}$$

Secondly, solutions of (77) satisfying (134) behave for $\zeta \to -\infty$ as

$$\varphi = -\frac{m+2}{3m} + Ee^{\zeta}, \tag{137}$$

where E is determined by the condition $\varphi(\zeta = 0) = 0$ (this can be done by virtue of the first of the invariances (79)). After the correct value of E has been found, the numerical integration proceedss towards $\zeta \to \infty$ where one necessarily arrives at a behaviour of the form

$$\varphi = H\zeta^{m/2} = f/R = HR^{m/2}\eta^{m/2}. \tag{138}$$

Once H is found numerically, R and $f_{-\infty}$ follow from the condition (see (133))

$$HR^{1+m/2} = 1, \tag{139}$$

whence

$$f_{-\infty} = -\frac{m+2}{3m} H^{2/(2+m)}. \tag{140}$$

The constant c, associated with the potential motion, is obtained from (134) and therefore the meridional motion is completely determined. Figure 11 shows φ and the dimensionless radial velocity component φ' for some values of m. It must be noted that, for $m = 1$, (77) has an exact solution corresponding to Schlichting's two-dimensional jet, $\varphi = \tanh \zeta$ (see the end of section 4.1.3), so that the inviscid stream function is not zero at both ends of the fan-jet in this case.

9. Transition from the one-cell to the two-cell solution and vortex breakdown

As shown in (**21**) (see also section 3.1), when $1 < m < 2$ and D is larger than a critical value D^* (Fig.3), there are two different one-cell solutions which are analogous to Long's solutions of type I and II. When $D < D^*$ and $1 < m < 2$, no single-cell solution exists, but there is a two-cell (type III) solution, which also exists for $D > D^*$. The bifurcation from I to III at decreasing

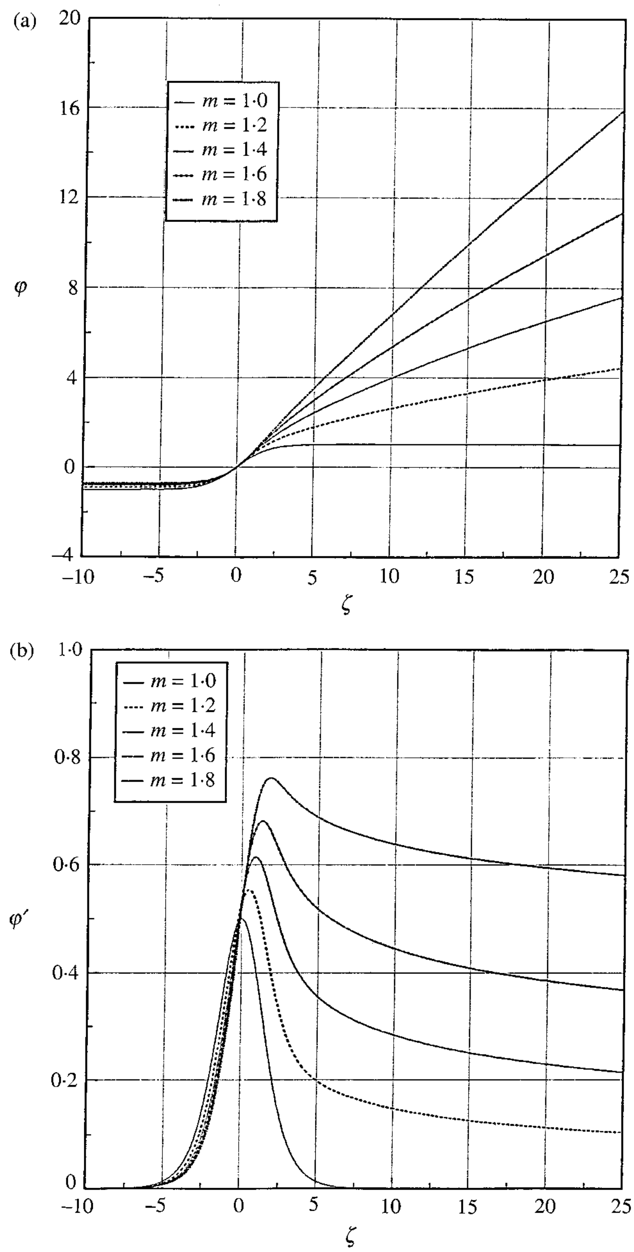

Fig. 11 Dimensionless meridional motion inside the fan-jet layer for some values of m. (a) Stream function $\varphi(\zeta)$. (b) Radial velocity component $\varphi'(\zeta)$

values of D may be represented in terms of the effect of this parameter on the radial velocity at the axis. Its values u_{1c} and u_{2c} for the one-cell (see (**21**)) and two-cell cases are, respectively,

$$\frac{u_{1c}}{K^2(\nu r)^{(m-2)/m}} = 2b^2 A_1, \tag{141}$$

$$\frac{u_{2c}}{[(\nu A)^{m/2} r^{m-4}]^{1/(m+2)}} = -\frac{6m(m-1) f_{-\infty} P_{m'-1}(1)}{(m+2)^2(1-x_s^2)^{2/(m+2)} P'_{m'-1}(x_s)}. \tag{142}$$

These dimensionless quantities are plotted in Fig. 12 for $m = 1{\cdot}6$ and $\alpha = \pi/2$. Note that u_{2c} is much smaller than u_{1c}:

$$\frac{u_{2c}}{u_{1c}} \sim \left(\frac{\nu r^{1-m}}{A^{m/4}}\right)^{4/m(m+2)} = \Delta^{2/m} \ll 1. \tag{143}$$

Accordingly, branch III in the sketch of the three solution branches given in Fig. 12(c) nearly coincides with the horizontal axis.

The main physical feature associated with the bifurcation from branch I into branch III when D drops below D^* is that the intense swirl and axial jet present near the axis for $D > D^*$ is radically expelled away from it and pushed into the outer cell when $D < D^*$. This metamorphosis of the flow is nearly identical to the axisymmetric manifestation of the vortex breakdown phenomenon arising in real flows, as earlier suggested by us (Fernandez de la Mora *et al.* (**39**); see also (**21**)). This similarity has also been discussed by Shtern and Hussain (**19**) for the particular case $m = 1$. However, as pointed out in the Introduction, the similarity between the model predictions and observations is far stronger for $m > 1$ than for $m = 1$, since now the bifurcation parameter D (or L) is precisely the one known to govern the real problem, while this is not the case in the highly degenerate case $m = 1$.

When $0 < m < 1$, two solutions exist for $D < D^*(m)$ and none for $D > D^*(m)$. But two-cell self-similar solutions do not exist in this case. This parameter range does not therefore seem to be relevant for real vortex flows, as indicated also by the fact that vortex breakdown is never observed below a critical value of the swirl parameter L (above a critical value of D)-always above a certain threshold of L (below a certain D). This is not surprising because vortex breakdown, and therefore a two-cell pattern, results when the swirl is too large.

10. Concluding remarks

We have considered incompressible conical flows at large Reynolds numbers with velocity fields of the form (1) in spherical polar coordinates. The particular case with $m = 1$, for which the complete incompressible Navier–Stokes equations can be written in similarity form, has been extensively studied in the literature. For $m \neq 1$, no conically similar solutions exist for the viscous problem, but they do exist for inviscid flows. We have analysed here these inviscid solutions in addition to several boundary and interior viscous layers matching with them, needed to describe high Reynolds number one- and two-cell conical flows. One of the reasons why these flows with $m \neq 1$ may be of interest is because their near axis viscous structure shows, for $1 < m < 2$, a behaviour more in agreement with observations of the vortex breakdown phenomenon than does the case $m = 1$. We have also discussed briefly their possible relevance to the motion inside Taylor cones. Finally, the present conical flows may be of interest as a reference to approximately model other swirling flows with nearly conical symmetry, such as the flows in tornadoes, swirl separators, etc.

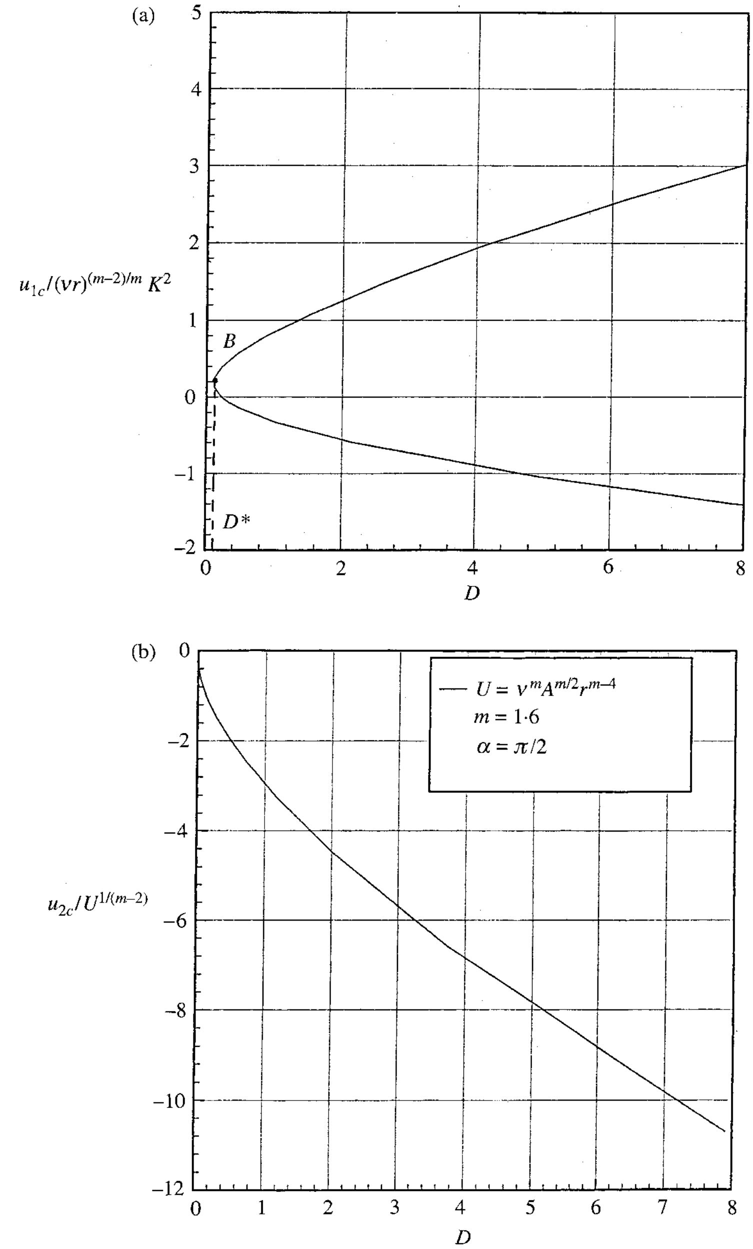

Fig. 12 (a) Dimensionless axial velocity at the axis $u_{1c}/K^2(\nu r)^{(m-2)/m}$ as a function of D corresponding to the one-cell case for $\alpha = \pi/2$ and $m = 1{\cdot}6$. (b) Dimensionless axial velocity at the axis $u_{2c}/[\nu^m A^{m/2} r^{m-4}]^{1/(m+2)}$ as a function of D corresponding to the two-cell case for $\alpha = \pi/2$ and $m = 1{\cdot}6$

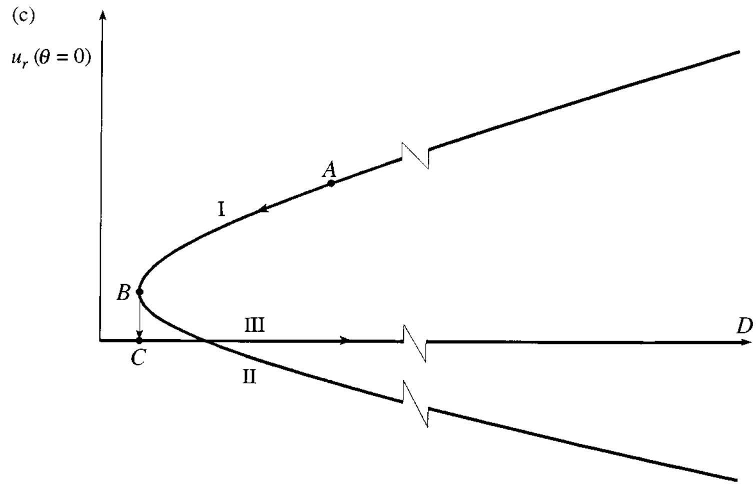

Fig. 12 (c) Sketch of the radial velocity at the axis as a function of D indicating the transition between the one- and two-cell regimes: as the swirl increases (D decreases) from a given value corresponding to a type I solution (point A, say), it eventually reaches the critical or folding swirl level (point B), after which the one cell solution breaks down and a transition towards a solution of type III is produced (point C, corresponding to a two-cell solution)

We have analysed exhaustively the parametric ranges for which one-cell similarity solutions exist for two particular boundary conditions at the cone surface: no velocity slip and a radial shear stress on the surface. These results are summarized in Figs 7 and 8 in terms of the parameter m, and in Fig. 3 in relation to the parameter D (related to the swirl parameter L through (63)). No loss of solutions is found as the other parameter of the problem, α, varies from 0 to $\pi/2$. As m, D and α vary slowly, the inviscid solutions change smoothly according to the results given in sections 2 and 7 (see Figs 2 and 9), except for the special values $m = 0$ and $m = 2$, where the inviscid behaviour may change abruptly (note that these values are usually associated with a change in the existence of the one-cell solution), and the folding values of D above or below which the one-cell solution is lost. When no similarity solution exists, it may be due to the axial boundary layer, to the surface boundary layer, or to both. When the cause is the surface boundary layer with a no-slip boundary condition at the surface, we find agreement with previous related works. For the cases with $1 \leq m < 2$ in which the failure of the one-cell conically similar solution is due to the axial boundary layer, we show the existence of a two-cell configuration to which we conjecture the one-cell solution jumps. This two-cell structure contains a potential inner cell, with no swirl and with much slower motion than the outer vortical inviscid cell, which resembles the bubble structure observed after breakdown of vortex flows, so that the transition from one- to two-cell structures is similar to this phenomenon for the present conically similar swirling flows. It should be emphasized here that, as discussed in section 7, the two-cell configuration considered is the only possible one allowed by the fan-jet and axial viscous layers. Conical flows with three or more cells are not allowed by the fan-jet layer, which can only match inviscid flows flowing away from the apex, as follows from the phase plane analysis of section 4.

As a final remark it should be mentioned that the present conical solutions are not valid near the origin, where they contain a singularity. In connection with this, viscous terms must be considered in the inviscid analysis near the origin ($r \to 0$) for $m > 1$, and, conversely, they must be taken into account for $r \to \infty$ when $m < 1$. The first case is perhaps the most interesting because the surface inflow towards the axis given by the boundary layer at the surface should turn upwards at the axis and re-emerge as the axial self-similar boundary layer flow in order for the solution to be valid. To check this, one has to consider the complete viscous problem near the origin, in a region where both surface and axial boundary layers merge (that is, from (75) or (97), $r \sim (\nu/K^m)^{1/(m-1)}$, $m > 1$), and analyse this 'effusing' problem (see, for example, Phillips (**40**)). Since similarity is lost in that region, one has to solve numerically the complete viscous equations, which is outside the scope of the present paper (see, for example, Barcilon (**41**) for a related problem). Analogously, for $m < 1$ one should retain viscous terms for very large r, where both viscous boundary layers merge, and check if the axial flow directed away from the apex re-emerges far from it as the surface flow. But, again, similarity is lost in those far regions, and the corresponding numerical analysis is outside the scope of the present paper.

Acknowledgements

This work has been supported by the Dirección General de Investigación Científica y Técnica of Spain, grants PB90-1023 and PB93-0974, by the US National Science Foundation grants CTS-9112601, CTS-9106619 and CTS-9319051, and by a NATO collaborative research grant, CRG950368. The authors thank Mr J. López-Herrera and Mr M. González for their valuable assistance in some calculations and drawings, respectively. Valuable comments from Drs Shtern and Gañán-Calvo are also acknowledged.

References

1. C. Y. Wang, *Ann. Rev. Fluid Mech.* **23** (1991) 159–178.
2. G. B. Jeffery, *Phil. Mag.* **29** (1915) 455–465.
3. G. Hamel, *Jahresbesicht Deutsch. Math. Verein,* **25** (1916) 34–60.
4. M. A. Goldshtik, F. Hussain and V. Shtern, *J. Fluid Mech.* **232** (1991) 521–566.
5. L. D. Landau, *Dokl. Ak. Nauk S.S.S.R.* **43** (1944) 286.
6. H. B. Squire, *Phil. Mag.* **43** (1952) 942–945.
7. M. A. Goldshtik, *Appl. Mat. Mech. (Sov.)* **24** (1960) 610–621.
8. C. Y. Yih, F. Wu, A. K. Garg and S. Leibovich, *Phys. Fluids* **25** (1982) 2147–2157.
9. A. F. Pillow and A. F. Paull, *J. Fluid Mech.,* **155** (1985) 327–358.
10. R. Paull, and A. F. Pillow, *ibid.* **155** (1985) 359–380.
11. V. Bojarevics, Ya. Freibergs, E. I. Shilova and E. V. Shecherbinin, *Electrically Induced Vortical Flows* (Kluwer, Dordrecht 1989) Chapter 2.
12. M. A. Goldshtik and V. M. Shtern, *J. Fluid Mech.* **218** (1990) 483–508.
13. C. Sozou, *ibid.* **244** (1992) 633–644.
14. G. I. Taylor, *Q. Jl Mech. appl. Math.* **3** (1950) 129–139.
15. R. L. Long, *J. Fluid Mech.* **11** (1961) 611–625.
16. O. R. Burggraf, K. Stewartson and R. J. Belcher, *Phys. Fluids* **14** (1971) 1821–1833.
17. —— and M. R. Foster, *J. Fluid Mech.* **80** (1977) 685–703.

18. M. G. Hall, *Ann. Rev. Fluid Mech.* **10** (1972) 195–218.
19. V. Shtern and F. Hussain, *Phys. Fluids* A **5** (1993) 2183–2195.
20. —— and ——, *J. Fluid Mech.* **309** (1996) 1–44.
21. R. Fernandez-Feria, J. Fernandez de la Mora and A. Barrero, *ibid.* **305** (1995) 77–91.
22. R. E. Spall, T. B. Gatski and C. E. Grosch, *Phys. Fluids* **30** (1987) 3434–3440.
23. P. S. Beran and F. E. C. Culik, *J. Fluid Mech.* **242** (1992) 491–527.
24. R. J. Belcher, O. R. Burggraf and K. Stewartson, *ibidh.* **52** (1972) 753–780.
25. I. Hayati, A. I. Bailey and Th. F. Tadros, *Nature* **319** (1986) 41–43.
26. A. M. Gañan-Calvo, private communication (1992).
27. J. Fernandez de la Mora and I.G. Loscertales, *J. Fluid Mech.* **260** (1994) 155–184.
28. A. M. Gañan-Calvo, J. Davila and A. Barrero, *J. Aerosol Sci.* **28** (1997) 249–275.
29. S. L. Bragg and W. R. Hawthorne, *J. Aero. Sci.* **17** (1950) 243–249.
30. M. Abramowitz and I. Stegun, *Handbook of Mathematical Functions* (National Bureau of Standards, Washington 1964).
31. G. W. Bluman and J. D. Cole, *Similarity Methods for Differential Equations* (Springer, Berlin 1974) 130–136.
32. A. J. Mestel, *J. Aerosol Sci.* **25** (1994) 1037–1047.
33. H. Schlichting, *Boundary Layer Theory* (McGraw–Hill, New York 1979) Chapters IX and XI.
34. J. C. Arrese and R. Fernandez-Feria, *Proc. 4th Ann. Conf. of the CFD Soc. of Canada* (Ottawa 1996) 697–704.
35. V. Shtern and A. Barrero, *Phys. Rev.* E **52** (1995) 627–635.
36. —— and ——, *J. Fluid Mech.* **300** (1995) 169–205.
37. C. W. Jones and J. Watson, in *Laminar Boundary Layer* (ed. L. Rosenhead; Dover, New York 1988).
38. K. Stewartson, *Proc. Camb. phil. Soc.* **50** (1954) 454–465.
39. J. Fernandez de la Mora, R. Fernandez-Feria and A. Barrero, *Bull. Am. Phys. Soc.* **37** (1992) 1708.
40. W. R. C. Phillips, *Phys. Fluids* **27** (1984) 2215–2220.
41. A. I. Barcilon, *J. Fluid Mech.* **27** (1967) 155–175.
42. G. K. Batchelor, *An Introduction to Fluid Dynamics* (University Press, Cambridge 1967).

APPENDIX A

Special conical solutions to Euler's equations

A.1 $m = 0$ *and other movements involving pure swirl*

In this case, equations (9) and (17) yield $F = 0$ everywhere, and the movement involves necessarily pure rotation. The well-known general solution to Euler's equation for this type of flow is an azimuthal velocity which depends only on the cylindrical variable $\sigma = r\sin\theta$. For the particular case $m = 0$ one finds $\Omega = 2C/\sin\theta$, $\Pi = -C^2/\sin^4\theta$. This solution, however, cannot be regularized at the axis. In fact, for a pure rotation, the complete Navier–Stokes equations with conical symmetry may be solved in closed form, yielding $u_\phi = Kr\sin\theta$ and $p/\rho = -K^2(r\sin\theta)^2/2$ as the unique solution regular at the axis, which is incompatible with the above inviscid solution for $m = 0$. In general, an inviscid pure swirl has the form (making $F = 0$ in (7), (8)): $\Omega = C(\sin\theta)^{m-1}$, $\Pi = [C^2/(2(m-2))](\sin\theta)^{2(m-2)}$. The corresponding azimuthal velocity, $u_\phi = C(r\sin\theta)^{m-2}$, has a regular derivative at the axis for $m \geq 3$ (notice that the limiting case $m = 3$ corresponds to the above viscous swirl).

A.2 $m = 1$

This case has been studied earlier in the literature because it corresponds to the only instance when the Navier–Stokes equations admit exact solutions with the kind of conical symmetry considered here (apart from a pure swirl). Equation (10) degenerates into the cylindrical potential vortex Ω = constant. Also, because the independent variable x does not enter explicitly into equation (16), F can be integrated completely for arbitrary α, K and D into

$$F^2 = 2(-K_1)^{1/2}(1 - x)(x - \cos\alpha)/(1 - \cos\alpha). \tag{A1}$$

This result has been reported in the literature, among others, by Paull and Pillow (**9**), (**10**) and by Goldshtik and Shtern (**12**). It follows also straightforwardly after ignoring the viscous terms (linear in F) from the general integral for the stream function in the well-known problem of the Landau jet (see, for example, Batchelor (**42**, section 4.6)):

$$F^2 - 2(1 - x^2)F' - 4xF = c_1x^2 + c_2x + c_3. \tag{A2}$$

Although this equation is valid only for the problem without swirl, because the extra terms associated with rotation are proportional to Ω', and Ω is constant in the inviscid region, the argument still holds for $\Omega \neq 0$.

The boundary layer analysis (near the axis and at the cone surface) for this case $m = 1$ is included in the range $0 < m < 2$. (The near-axis layer constitutes Long's vortex (**15**).)

A.3 $m = 2$

In this case, (7) and (9) yield a linear equation for F which can be integrated exactly into

$$F = -\frac{K^2}{4}\left[\frac{(1 - x)(x - \cos\alpha)}{1 + \cos\alpha} + \frac{1 - x^2}{2}\ln\frac{(1 + x)(1 - \cos\alpha)}{(1 - x)(1 + \cos\alpha)}\right]. \tag{A3}$$

Notice that non-trivial solutions exist only for non-swirling flows ($K \neq 0$). The associated behaviours at the axis and at the cone surface are

$$x \to 1: \quad \Psi \to -(Kr\theta)^2 \ln\theta/4, \tag{A4}$$

$$u_\phi \to K^2(-\ln\theta)^{1/2}/2, \quad p/\rho \to -K^4(\ln\theta)^2/8; \tag{A5}$$

$$x \to x_\alpha \equiv \cos\alpha: \quad \Psi \to \frac{K^2}{2}r^2\frac{x_\alpha - x}{1 + x_\alpha}, \tag{A6}$$

$$u_\phi \to K^2\frac{(x - x_\alpha)^{1/2}}{(1 + x_\alpha)(1 - x_\alpha)^{1/2}}, \quad p/\rho \to -K^4/8(1 + x_\alpha)^2. \tag{A7}$$

At the cone surface, $u_\phi/u_r \sim (x - x_\alpha)^{1/2} \to 0$, and the pressure gradient term is of the same order as the convective term in the boundary layer at the cone surface, as in the case $m > 2$ (section 2.1.3). Thus, the analysis given in section 5 is valid also for $m = 2$; one only has to use $\gamma = [2(1 + \cos\alpha)]^{-1}$ instead of (99). On the contrary, the near axis behaviour is analogous to that of the range $0 < m < 2$, with the only difference that now the singularity has a logarithmic nature. It may be shown that this singularity can only be regularized by a viscous boundary layer when the near-axis inviscid meridional flow is directed away from the origin, as occurs for $0 < m < 2$ (see section 3.1). Since we showed in section 5 that a solution for $m \geq 2$ only exists if the near-surface motion is directed away from the cone tip, it must be concluded that no solutions exist corresponding to an inviscid conical flow with $m = 2$.

APPENDIX B

Solutions for $K = 0$

For swirl-less inviscid flows ($K = 0$), instead of the dimensionless variable (21) one may use

$$Y = F/|K_1|^{m/4}, \tag{B1}$$

which transforms (16) into

$$mY'' + (m-1)m^2 Y/(1-x^2) = \pm Y^{1-4/m}, \tag{B2}$$

where the right-hand side is negative for $m < 2$, and positive for $m > 2$ (notice that $K_1 < 0$ for $m < 2$ and $K_1 > 0$ for $m > 2$, see (15); for $m = 2$, see Appendix A.3). When K_1 is also zero, the inviscid flow is potential, and what follows is not valid (see section 2.2).

B.1 *$m < 0$ and $m > 2$*

Similarly to the case $K \neq 0$ (sections 2.1.1 and 2.1.3), the solution of (B2) approaches the axis and the cone surface as

$$Y \to a'(1-x), \quad x \to 1, \tag{B3}$$

$$Y \to B'(x - \cos\alpha), \quad x \to \cos\alpha, \tag{B4}$$

where $a' > 0$ is an arbitrary constant which fixes the cone angle α and the constant B' for each m, after integrating numerically (B2) starting at the axis as in (B3). According to (B3), the inviscid solution is regular at the axis, so that no viscous boundary layer is needed there (see section 3.2). Near the cone surface, the velocity and pressure fields behave as

$$\Psi \to |K_1|^{m/4} B' \sin\alpha\, r^m (\alpha - \theta), \quad \frac{p}{\rho} \to -|K_1|^{m/2} \frac{B'^2}{2} r^{2(m-2)}. \tag{B5}$$

Therefore, the pressure gradient is not negligible inside the surface boundary layer, and the analysis given in section 5 is valid for this case $K = 0$, provided one uses

$$\Delta = \left(\nu/|K_1|^{m/4}\right)^{1/2} \; r^{(1-m)/2}, \tag{B6}$$

instead of (97), and $\gamma = B'$ instead of (99). (Notice that, since the inviscid free constant D has disappeared from the problem, the numerical constant B' depends only on the cone angle α and on m.) Figures 5 and 6 are thus also valid for $K = 0$. For a shear stress boundary condition on the cone surface of the form (93), where n is related to m through (114), the intensity of the meridional motion $|K_1|$ is related to the shear stress constant Γ_n and the other parameters of the problem by

$$|K_1|^{m/4} = \frac{1}{B'(\alpha, m)} \left(\frac{2j\Gamma_n^2}{(1+m)\nu\rho^2} \right)^{1/3}, \quad m \neq -1 \quad (n \neq -5), \tag{B7}$$

$$|K_1|^{1/4} = B'(3\nu)^{1/3} (\rho/\Gamma_{-5})^{2/3}, \quad m = -1 \quad (n = -5) \quad ; \tag{B8}$$

expression (B7) is obtained from (116) by just interchanging K^m with $|K_1|^{m/4}$, and setting $\gamma = B'$.

B.2 $0 < m < 2$

As in the case $K \neq 0$, in this range the analysis of the inviscid solution near the singular end points is simplified, eliminating the non-integer powers in (B2) by defining the variable

$$y = (m/\sqrt{2}) Y^{2/m} = F^{2/m}/(-2K_1/m^2)^{1/2}, \tag{B9}$$

which transforms that equation into

$$yy'' + \frac{m-2}{2} y'^2 + \frac{2(m-1)}{1-x^2} y^2 + 1 = 0. \tag{B10}$$

The analysis of the solution near the axis is similar to that given in section 2.1.2. One has

$$y \simeq \left(\frac{2}{2-m}\right)^{\frac{1}{2}} (1-x) \left[1 + A'(1-x)^{2-m} + \frac{B'}{1-x} \right], \qquad 1 - x \ll 1. \tag{B11}$$

Near the cone surface, a first integration of (B10) yields

$$y'^2 = \frac{2}{2-m} + 4G'y^{2-m} - \frac{4(m-1)}{m\sin^2\alpha}y^2 + O(y^3), \tag{B12}$$

where A', B' and G' are arbitrary constants. The axis ($x = 1$) is a saddle point which can only be reached through the family of trajectories corresponding to $B' = 0$ in (B11), while the cone surface ($x = \cos\alpha$) is a nodal point. Accordingly, given a value of A' for each m, the numerical integration of (B10) is started near the axis as in (B11) with $B' = 0$, and proceeds until behaviour (B12) is reached for some value of the cone angle $\alpha = \alpha(A', m)$, with $G' = G'(A', m)$. The resulting functions $y(\theta)$ are qualitatively similar to those depicted in Fig.2(b), so that they are not plotted.

The velocity and pressure fields when approaching both the axis and the cone surface are

$$x \to 1: \quad \Psi \to \left(\frac{-K_1}{m^2(2-m)}\right)^{m/4} (r\theta)^m, \tag{B13}$$

$$\frac{p}{\rho} \to \left(\frac{-K_1}{2-m}\right)^{m/2} \frac{r^{2(m-2)}}{2m^{m-1}}[2^m(3-m)A' + m\theta^{2(m-1)}]; \tag{B14}$$

$$x \to \cos\alpha: \quad \Psi \to \left(\frac{-4K_1\sin^2\alpha}{m^2(2-m)}\right)^{m/4} r^m(\alpha-\theta)^{m/2}, \quad \frac{p}{\rho} \to -\frac{(-2K_1)^{m/2}G'}{2m^{m-2}}r^{2(m-2)}. \tag{B15}$$

The pressure gradient is thus negligible in the boundary layer at the cone surface, and its structure is that given in section 4. The analysis in the self-similar variables given there remains the same, provided one changes the constants appearing in the angular thickness $\Delta(r)$ (equation (75)):

$$\Delta^{m+2} = [(B\nu)^2(\sin\alpha)^{2(1-m)}(m^2(m-2)/4K_1)^{m/2}]r^{2(1-m)}. \tag{B16}$$

For a shear-driven flow, instead of (95) one has

$$-K_1 = \frac{m^2(2-m)}{4}B^{4/m}\left(\frac{\Gamma_n}{\rho}\right)^{2(m+2)/3m}(\nu^{1/3}\sin\alpha)^{4(1-m)/m}, \tag{B17}$$

where m is related to n through (94). As expected, this relation fixes the intensity of the inviscid meridional motion $|K_1|$ as a function of the shear parameters, the cone angle, and the physical properties of the liquid.

The inviscid flow should be regularized at the axis by a viscous boundary layer analogous to that considered in (**21**) (see section 3.1), but the governing equations are now much simpler because now there is no swirl and, consequently, the pressure gradient is negligible inside the boundary layer (compare (B14) with u_r^2 obtained from (B13)). The structure of this near-axis boundary layer is given by just one ordinary differential equation (the r-momentum equation) which may be written as

$$\frac{2-m}{m}f'^2 + ff'' + 2(\xi f'')' = 0, \tag{B18}$$

where

$$\Psi \equiv \nu r f(\xi), \tag{B19}$$

and the primes denote differentiation with respect to ξ, where

$$\xi \equiv \left(\frac{\theta}{\Delta}\right)^2, \quad \Delta^m = r^{1-m}\nu\left(\frac{m^2(2-m)}{-K_1}\right)^{m/4} \tag{B20}$$

($\Delta(r)$ is obtained by comparing (B19) with (B13), taking into account that $f \sim \xi^{m/2}$ as $\xi \to \infty$). At the

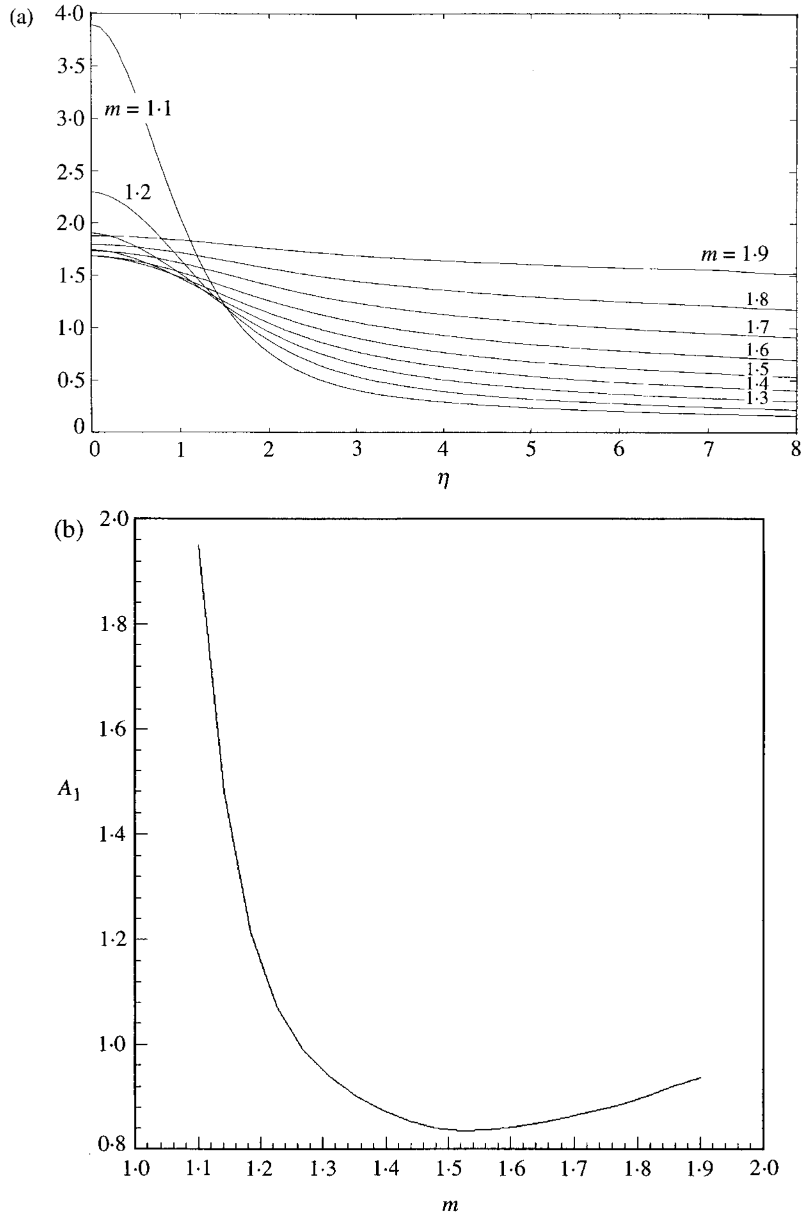

Fig. B1 (a) Radial velocity profiles, $r\Delta(r)u_r/\nu = f'(\eta)/\eta$, ($\eta \equiv \theta/\Delta(r) = \xi^{1/2}$) in the axial boundary layer for $K = 0$, for several values of m ($1 < m < 2$). (b) Constants $A_1(m)$ (equation (B21)) for which the axial boundary layer equation with $K = 0$ has a solution axis, the behaviour of the solution is the same as in (**21**), but with $g_0 = 0$. The series may now be summed as

$$f \simeq A_1\xi \, \frac{1 + \dfrac{m-1}{6m} A_1\xi}{1 - \dfrac{m-4}{12m} A_1\xi}, \quad \xi \ll 1, \tag{B21}$$

where A_1 is a free constant ($2A_1$ is the non-dimensional axial velocity at the axis). As $\xi \to \infty$, one has

$$f \to l\xi^{m/2} + C_1\xi^{(m-2)/2} + C_2 \exp[(-l/m)\xi^{m/2}], \quad l = \pm 1, \tag{B22}$$

where C_1 and C_2 are arbitrary constants. Similarly to the case $K \neq 0$, there is no solution for a near-axis inviscid flow directed towards the origin ($l = -1$) because the exponential term in (B22) diverges, C_2 must be equal to zero, and there are not enough degrees of freedom to cancel that divergence. For $m = 1$, equation (B18) may be integrated once, giving

$$ff' + 2\xi f'' = C, \tag{B23}$$

where $C = 0$ to meet the condition at the axis. A solution of this equation which satisfies (B21) is

$$f = \frac{A_1\xi}{1 + A_1\xi/4}, \tag{B24}$$

which corresponds to the Schlichting axisymmetric jet (see, for example, Schlichting (**33**)). However, this solution does not satisfy the boundary condition at infinity. Therefore, for $m = 1$ (and both $l = \pm 1$), there is no solution without swirl, as was already shown in (**21**) (see also Fig. 3). Numerically, one finds that solutions with $l = +1$ do not exist for $m < 1$. When $m > 1$ (of course, $l = +1$), there is only one value of $A_1(m)$ for which the boundary condition at infinity (B22) is satisfied. Obviously, these results about the existence of the solutions are in agreement with those in the limit $D \to \infty$ (corresponding to $K = 0$), summarized in section 3.1 (see Fig. 3, where it is clear that swirl-less flows only exist for $m > 1$). Aside from the boundary layer structure, which now is obtained by integrating just one ordinary differential equation, the only new relevant result of the present near-axis boundary layer analysis in relation to that of (**21**) is that now there is just one solution for each value of m in the range $1 < m < 2$, $l = +1$. The values of $A_1(m)$, and some radial velocity profiles, $r\Delta^2 u_r/\nu = 2f'(\xi)$, are plotted in Fig. B1.

APPENDIX C

Swirl in the boundary layer at the cone surface

Here we consider the azimuthal motion confined in the viscous boundary layer near $\theta = \alpha$, which regularizes the inviscid swirl (equations (30), (46) and (54)). The azimuthal velocity component u_ϕ does not enter into the radial momentum equation because, as seen in section 2, $u_\phi/u_r \to 0$ as $\theta \to \alpha$ in the inviscid flow for all values of m. It will be shown that the equation governing u_ϕ in this boundary layer (which is linear) allows the matching of a zero azimuthal shear stress $\tau_{\theta\phi}$ at the surface with the inviscid solution for any value of K, so that the inviscid swirl, if it exists, is not due to $\tau_{\theta\phi}$. In relation to the no-slip boundary condition on the cone surface, it will be shown that, for the cases for which the meridional motion is compatible with it, that is, for $m \leq -1$ and $m > 2$, only the case $m = -1$ is not compatible with a zero azimuthal velocity at the cone surface.

The azimuthal momentum equation in the boundary layer near $\theta = \alpha$ is

$$u_r \frac{\partial u_\phi}{\partial r} + \frac{u_\theta}{r}\frac{\partial u_\phi}{\partial \theta} + \frac{u_\phi u_r}{r} = \frac{\nu}{r^2}\frac{\partial^2 u_\phi}{\partial \theta^2}. \tag{C1}$$

We shall consider separately the cases $0 < m < 2$, and $m < 0$, $m > 2$, whose meridional boundary layers have been considered in sections 4 and 5, respectively.

C.1 $0 < m < 2$

Defining

$$u_\phi = W r^p h(\eta), \tag{C2}$$

where the matching condition (46) together with (75) (provided that $h(\eta) \to (-\eta)^{(m-1)/2}$ as $\eta \to -\infty$) yields W and p as

$$p = \frac{2m-5}{m+2}, \quad W^{m+2} = K^{3m}(Q/m)^{2(m-1)}(\sin\alpha)^{m-4}(B\nu)^{m-1}, \tag{C3}$$

and taking into account (76) for u_r and u_θ, (C1) becomes

$$h'' + \frac{3m}{m+2} f h' + \frac{3(1-m)}{m+2} f' h = 0, \tag{C4}$$

with $f(\eta)$ known from the analysis of section 4. As $\eta \to \infty$, f behaves according to (94), and the above equation gives

$$h \to E_1(-\eta)^{(m-1)/2} + E_2 \exp\left[-\frac{9m}{(m+2)^2} B(-\eta)^{(m+2)/2}\right], \quad \eta \to -\infty, \tag{C5}$$

where E_1 and E_2 are free constants, but E_1 has been selected equal to unity according to the matching condition (C3). Thus, the point at infinity is a node which attracts all the trajectories to the behaviour given by the first term in the above equation. At the cone surface ($\eta = 0$), f is given by (83) and

$$h = e_0 + e_1\eta + \frac{3(m-1)}{2(m+2)} c_1 e_0 \eta^2 + \ldots, \tag{C6}$$

so that one has two degrees of freedom, e_0 and e_1, to meet the boundary condition at the surface and to fix $E_1 = 1$. For the present case $0 < m < 2$ the meridional motion analysed in section 4 is not compatible with a no-slip boundary condition on the cone surface; therefore only the case of a shear stress boundary condition is considered here. In particular, one is interested in solutions with zero azimuthal shear stress on the cone surface, that is, $\tau_{\theta\phi} = 0$ at $\theta = \alpha$, implying $e_1 = 0$. Thus one starts the numerical integration of (C4) at $\eta = 0$ with $e_1 = 0$ and a given value of e_0 (say $e_0 = 1$) and proceeds towards $\eta \to -\infty$, obtaining a value for E_1. Since the equation is linear, a simple shift in e_0 yields the required value of $E_1 = 1$.

C.2 $m < 0$ *and* $m > 2$

Although the boundary layer analysis of section 5 is valid for $m < 0$ and $m > 2$, we showed there that the solutions are physically meaningful for $m \le -1$ and $m > 2$. Using the same notation (C2), the matching conditions (30) and (54), assuming that $h(\eta) \to (-\eta)^{(m-1)/m}$ as $\eta \to -\infty$, yield

$$p = \frac{m^2-2m-1}{2m}, \quad W = \gamma^{(m-1)/m} K^{(m+1)/2} \nu^{(m-1)/2m} (\sin\alpha)^{-1/m}, \tag{C7}$$

where γ is given by (95). Substituting into (C1), one obtains

$$h'' + \frac{1+m}{2} f h' + \frac{1-m^2}{2m} f' h = 0, \tag{C8}$$

where $f(\eta)$ is known from the analysis of section 5.

For $m = -1$, the above equation becomes simply $h'' = 0$, whose general solution is the linear function $h = e_0 + e_1\eta$, e_0 and e_1 being free constants. However, this solution cannot match the inviscid behaviour $h \to (-\eta)^2$ as $\eta \to -\infty$.

For $m \neq -1$, the situation is similar to that considered in C.1, but now a no-slip boundary condition must be considered. Near the cone surface, using (83) (notice that the behaviour as $\eta \to 0$ is the same for the meridional motion in both cases considered in sections 4 and 5), equation (C8) yields

$$h = e_0 + e_1\eta + \frac{m^2-1}{4m}c_1 e_0 \eta^2 - \left[\frac{m+1}{12m}c_1 e_1 + \frac{1-m^2}{6m}c_2 e_0\right]\eta^3 + \ldots, \quad |\eta| \ll 1. \tag{C9}$$

On the other hand, the behaviour of $h(\eta)$ as $\eta \to -\infty$ is

$$h \to E_1(-\eta)^{(m-1)/m} + E_2 \exp\left[\left(\frac{(m^2-1)j\gamma}{2m}\right)^{1/2}\eta\right], \quad \eta \to -\infty, \tag{C10}$$

where E_1 and E_2 are arbitrary constants, but we fix $E_1 = 1$ according to the matching condition (C7), $j = -1$ for $m < -1$ and $j = +1$ for $m > 2$ (see section 5). The numerical integration procedure is thus the same as given in C.1. For a no-slip boundary condition, c_1 and e_0 are zero in (C9), and one has the constant e_1 as a degree of freedom to select the solution with $E_1 = 1$.

APPENDIX D

Pressure and azimuthal velocity in the fan-jet layer

After the meridional velocity components u_r and u_θ are obtained inside the fan-jet layer (section 8), the pressure and azimuthal velocity fields can be found by integration of the momentum equations in the θ- and ϕ-directions:

$$u_r\frac{\partial u_\phi}{\partial r} + \frac{u_\theta}{r}\frac{\partial u_\phi}{\partial \theta} + \frac{u_r u_\phi}{r} = \frac{\nu}{r^2}\frac{\partial^2 u_\phi}{\partial \theta^2}, \tag{D1}$$

$$u_r\frac{\partial u_\theta}{\partial r} + \frac{u_\theta}{r}\frac{\partial u_\theta}{\partial \theta} + \frac{u_r u_\theta}{r} - \frac{\cot\theta_s u_\phi^2}{r} = -\frac{1}{r}\frac{\partial p/\rho}{\partial \theta} + \frac{\nu}{r^2}\frac{\partial^2 u_\theta}{\partial \theta^2} + \frac{2\nu}{r^2}\frac{\partial u_r}{\partial \theta}. \tag{D2}$$

To that end, one defines the self-similar variables $\beta(\zeta)$ and $\omega(\zeta)$ as

$$\frac{p}{\rho} = \frac{\nu^2 R^2}{(m+2)A_2^2} r^{2(m-4)/(m+2)}\beta(\zeta), \tag{D3}$$

$$u_\phi = \frac{\nu S(1-x_s^2)^{1/4}}{(m+2)^{1/2}x_s^{1/2}A_2^{3/2}} r^{(2m-5)/(m+2)}\omega(\zeta), \tag{D4}$$

where the constant S in (D4) will be chosen to simplify the matching condition with the outer cell. In terms of β, ω and φ, equations (D1) and (D2) read

$$(m+2)\omega'' = 3(m-1)\omega\varphi' - 3m\varphi\omega', \tag{D5}$$

$$\beta' = \frac{S^2\omega^2}{R^3} - \frac{9m^2}{m+2}\varphi\varphi' - \frac{2(m-1)\zeta}{m+2}[3m\varphi\varphi'' - 2(m-1)\varphi'^2] - [(5m-8)\varphi'' + 2(m-1)\zeta\varphi''']. \tag{D6}$$

Since φ is already known, ω can be obtained from (D5). One boundary condition for ω is provided by (119), namely

$$\omega(\zeta \to \infty) = \zeta^{(m-1)/2}, \tag{D7}$$

where S has been chosen as

$$S = \frac{m(m+2)^{1/2}x_s^{1/2}}{I^{1/2}(1-x_s^2)^{1/2}R^{(m-1)/2}}. \tag{D8}$$

Matching u_ϕ in both the fan-jet and the potential cell ($\zeta \to -\infty$) requires $\omega(-\infty) = 0$; then, by substituting (137) into (D5) one finds that

$$\omega(\zeta \to -\infty) = C_\omega e^\zeta, \tag{D9}$$

which is the second boundary condition for ω. Since (D5) is a linear equation, the numerical integration

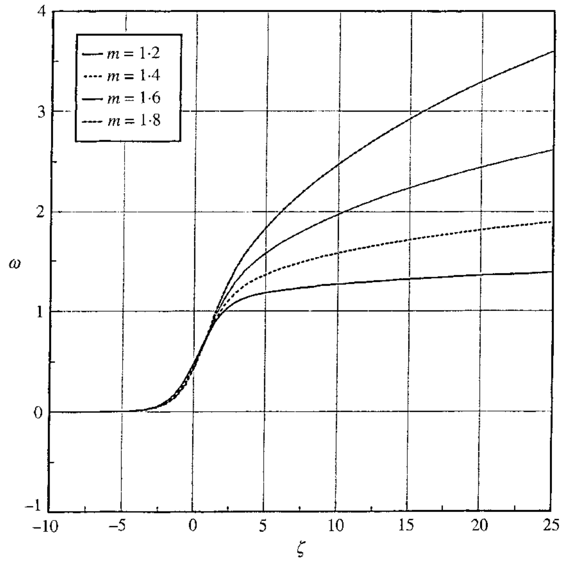

Fig. D1 Dimensionless swirl velocity component ω as a function of the dimensionless coordinate ζ in the fan-jet for some values of m

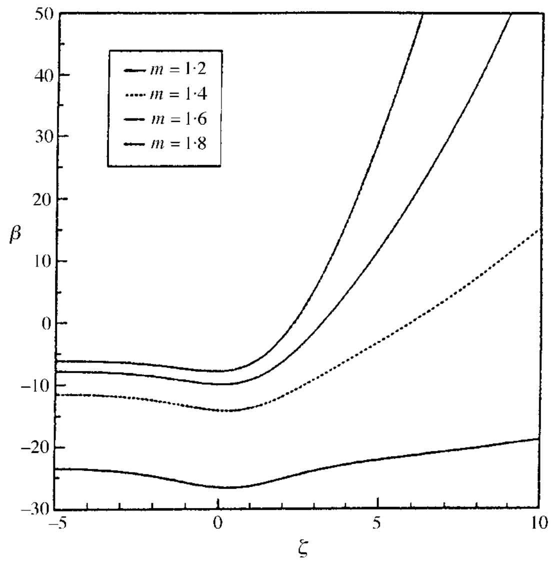

Fig. D2 Dimensionless pressure β as a function of the dimensionless coordinate ζ in the fan-jet for $\theta_s = \pi/3$ and some values of m

can be started at $\zeta \to -\infty$ with an arbitrary value of C_ω, say $C_\omega = 1$; then, the value of C_ω is rescaled to satisfy condition (D7). Dimensionless swirl velocity profiles $\omega(\zeta)$ are plotted in Fig. D1 for several values of m.

Once φ and ω are known, (D6) is solved subject to the inner-cell matching condition (60) which, in terms of the self-similar variables, reads

$$\beta(\zeta \to -\infty) \to -\frac{2(m-1)^2}{m+2}\left[\frac{P_{m'-1}(x_s)}{P'_{m'-1}(x_s)}\right]^2 - \frac{m+2}{2}. \tag{D10}$$

As $\zeta \to \infty$, β behaves as

$$\beta(\zeta \to \infty) \to \frac{m(m+2)}{R^{m+2}}\left[\frac{x_s}{(1-x_s)^2 I} - \frac{1}{2}\right]\zeta^m, \tag{D11}$$

thus recovering the outer-cell behaviour (120) with the constant $G = 0$. Figure D2 shows values of the dimensionless pressure β across the fan-jet for $\theta_s = \pi/3$ and several values of m.